Journal of Nanobiotechnology

RESEARCH

Open Access

Exploring the link between M1 macrophages and EMT of amniotic epithelial cells: implications for premature rupture of membranes

Yuhua Gao[1,4], Yanan Zhang[2], Ningning Mi[3], Wang Miao[1], Jingmiao Zhang[1], Yize Liu[1], Zhikun Li[1], Jiaxun Song[1], Xiangchen Li[3*], Weijun Guan[4*] and Chunyu Bai[1,4*]

Abstract

Background Despite increasing evidence supporting the role of an amniotic epithelial-mesenchymal transition (EMT) in the premature rupture of membranes (PROMs), it remains unclear if extracellular vesicle (EV) derived from M1 macrophages play a critical role in triggering the EMT of amniotic epithelial cells (AECs).

Results This study revealed that under inflammatory conditions, EV-miR-146a/155 from M1 macrophages could trigger EMTs and MMP-9 transcription in AECs, elevating the risk of PROM in both mice and humans. Introduction of EV-miR-155 led to inhibition of Ehf expression and reduced E-cadherin transcription in AECs. Meanwhile, EV-miR-146a activated the β-catenin/Tcf7 complex to promote the transcription of Snail, MMP-9, and miR-146a/155, inducing EMTs. Subsequently, EMT induction in AECs is associated with a loss of epithelial characteristics, disruption of cellular junctions, widening of intercellular spaces, and diminished biomechanical properties of the amniotic membrane.

Conclusion Inflammatory stimulation prompts the polarization of macrophages in amniotic fluid into the M1 type, which subsequently secrete EVs laden with inflammatory miRNAs. These EVs trigger the EMT of AECs, causing the loss of their epithelial phenotype. Consequently, the biomechanical properties of the amnion deteriorate, ultimately leading to its rupture, posing risks relevant to pregnancy complications such as premature rupture of membranes. The results of this study provide insights into the pathogenesis of PROM and will aid in treatment development.

Keywords Amniotic epithelial cells, Extracellular vesicles, Macrophages, Epithelial-mesenchymal transition

*Correspondence:
Xiangchen Li
xcli863@zafu.edu.cn
Weijun Guan
guanweijun@caas.cn
Chunyu Bai
chunyu_bai@hotmail.com
[1]Precision Medicine Laboratory for Chronic Non-communicable Diseases of Shandong Province, Institute of Precision Medicine, Jining Medical University, No.133 Hehua Road, Jining, Shandong 272067, P. R. China
[2]Department of Obstetrics, Affiliated Hospital of Jining Medical University, Jining 272000, P. R. China
[3]College of Animal Science and Technology, College of Veterinary Medicine, Zhejiang A&F University, No. 666, Wusu Road, Lin'an 311300, P. R. China
[4]Institute of Animal Sciences, Chinese Academy of Agricultural Sciences, No.2 Yuanmingyuan West Street, Haidian District, Beijing 100193, P. R. China

© The Author(s) 2025. **Open Access** This article is licensed under a Creative Commons Attribution-NonCommercial-NoDerivatives 4.0 International License, which permits any non-commercial use, sharing, distribution and reproduction in any medium or format, as long as you give appropriate credit to the original author(s) and the source, provide a link to the Creative Commons licence, and indicate if you modified the licensed material. You do not have permission under this licence to share adapted material derived from this article or parts of it. The images or other third party material in this article are included in the article's Creative Commons licence, unless indicated otherwise in a credit line to the material. If material is not included in the article's Creative Commons licence and your intended use is not permitted by statutory regulation or exceeds the permitted use, you will need to obtain permission directly from the copyright holder. To view a copy of this licence, visit http://creativecommons.org/licenses/by-nc-nd/4.0/.

Introduction

The epithelial-mesenchymal transition (EMT) is a biological process involving multiple molecular events, during which polarized epithelial cells acquire mesenchymal cell phenotypes. EMT plays a critical role in the proliferation and metastasis of cancer cells [1–3], and is also required for the organogenesis of various mammalian tissues, such as hair follicles, skin, teeth, mammary glands, prostate, lungs, and kidneys [4]. Amniotic epithelial cells (AECs) collected from the inner amnion epithelium, representing a type of stem cell that expresses some of the same markers as embryonic stem cells, and can develop into cells for all three germ layers [5–8]. The epithelial phenotype of AECs helps to strengthen the amnion and maintain pregnancy. EMT has been observed in AECs from the amnion during vaginal delivery, including natural labor (NL) and preterm birth. Our previous study revealed that AECs spontaneously undergo EMT when cultured in vitro, which enhances the efficiency of neuron differentiation [9]. These data prompted further investigation to determine whether the epithelial phenotype of AECs is related to fetal development in vivo.

The generation of a small sterile rupture in the mouse amniotic membrane using a 26 G needle was previously found to facilitate EMT in AECs via the action of inflammatory cytokines (interleukin-1β and TNF) released by the recruited macrophages [10] and is associated with rupture healing. Large ruptures can also be associated with a poor prognosis because of the absence of matrix deposition and the expression of matrix metalloproteinase 9 (MMP 9). MMP 9 is secreted by AECs and stromal cells in response to inflammatory cytokines and plays a crucial role in the degradation of the extracellular matrix of fetal membranes under both normal and pathological conditions [11, 12]. The recruitment of macrophages by bacteria-induced inflammatory reactions and their pathological effects on the rupture of fetal membranes remain poorly understood. Janzen et al. reported that amniotic cells show an increase in the number of mesenchymal cells relative to epithelial cells in the amnions of vaginal deliveries, including natural labor and preterm birth. In contrast, the amnions from cesarean sections contained a significantly lower percentage of mesenchymal cells. Moreover, the mesenchymal phenotype of AECs increased after TNF-α or EMT inducer treatments, which decreased the time and mechanical pressure required for amnion rupture; however, maintaining the epithelial phenotype was necessary to strengthen the amnion. These reports suggest that inflammatory factors and EMT inducers promote the EMT of amniotic cells, which increases the risk of amniotic rupture, and emphasize the critical role of EMT in premature rupture of membranes (PROMs) pathophysiology [13, 14]. However, the specific EMT trigger in AECs located in the lining of the amniotic epithelium in PROMs remains unknown.

Extracellular vesicles (EVs) are nanometer-scale vesicles (50–200 nm in diameter), exhibit "dish" shapes [15], which are secreted by various cell types, contain cellular proteins, lipids, DNAs, and RNAs, and act as mediators of intercellular communication [16]. EVs have been identified in saliva [17], plasma [18], urine [19], amniotic fluid [20], malignant ascites [21], cerebrospinal fluid [22], and bronchial alveolar lavage fluid [23], all of which have been exploited as novel reservoirs for disease biomarker discovery in previous studies [24–26]. Amniotic fluid serves as a cushion for the growing fetus and facilitates the exchange of nutrients with the mother. EVs derived from amniotic fluid have been identified as key players in the pathogenesis of PROM [27, 28]. Specifically, the upregulation of miR-162 in circulating EVs has been linked to the activation of apoptosis and the NF-κB pathway, both of which are known to be associated with PROM [29]. Additionally, exosomes from amniotic fluid have been found to contain elevated levels of pregnancy zone protein in cases of PROM [30]. Furthermore, under oxidative stress conditions, AECs have been observed to release a significant quantity of EVs into the amniotic fluid during the inflammatory response [31]. However, there is currently a lack of research on the regulatory interactions between EVs derived from M1 macrophages in amniotic fluid and AECs during PROM. In this study, lipopolysaccharide (LPS)-induced PROMs in a mouse model were used to investigate the role and origin of related EVs in the amniotic fluid by influencing the EMT of AECs. The results showed that macrophages were recruited to the uterus and amniotic fluid, resulting in the release of inflammatory EVs that increased the expression of EV-miRNAs in the amniotic fluid to trigger EMT and activate the expression of MMP-9 in AECs. The molecular mechanisms underlying the packaging and transport of EV-miRNAs from macrophages to AECs were also elucidated. The results were further validated in clinical PROM samples caused by bacterial vaginosis.

Results

EMTs in AECs and recruited macrophages from LPS-treated PROM mice

In this study, pregnant mice were divided into three groups: LPS-induced PROMs, natural labor (NL), and cesarean section (CS), to analyze EMTs in AECs. EMT was first verified in the mouse amnion using immunofluorescence and then in fresh AECs using western blot analysis. The mesenchymal markers (N-cadherin) were significantly increased compared with the epithelial markers (E-cadherin) in vaginal deliveries, including LPS-induced PROMs and natural labor (NL). Conversely, cesarean sections (CS) (Fig. 1A) showed the opposite

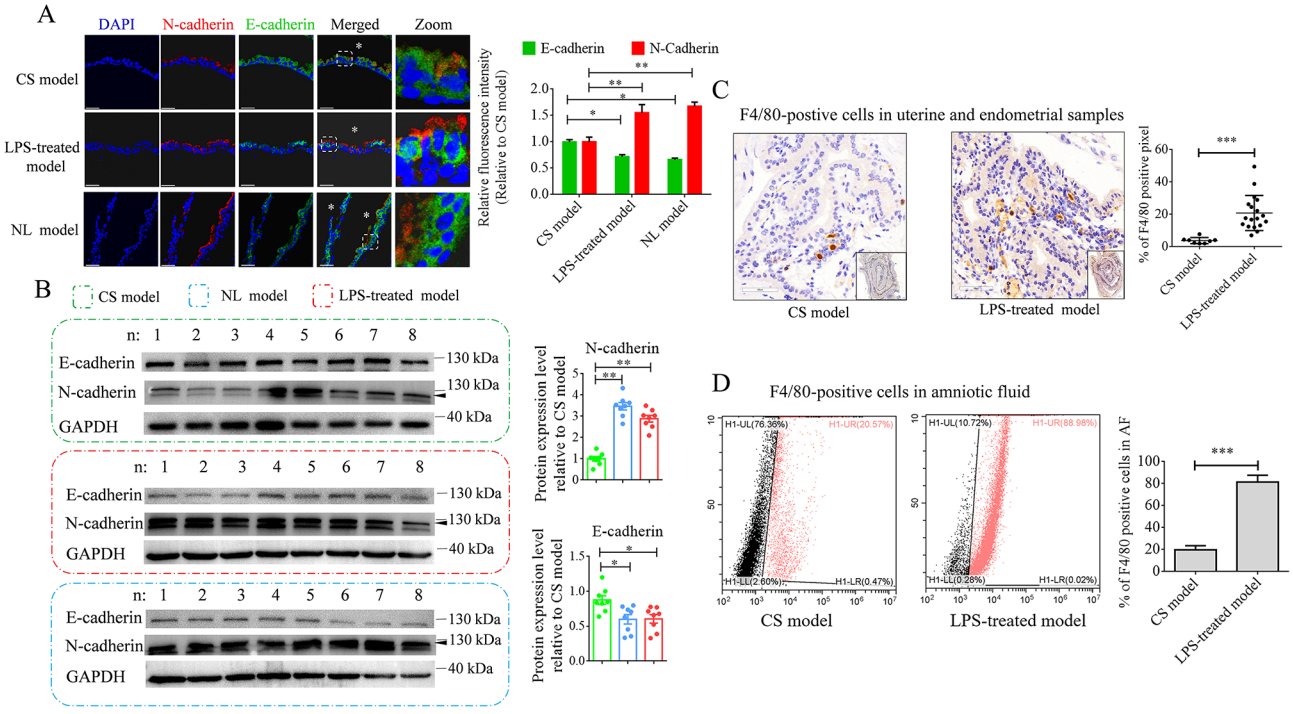

Fig. 1 Characterization of the amniotic membrane from the LPS-treated, natural labor (NL), and cesarean section (CS) models. (**A**) EMT key markers of native AECs were analyzed using immunofluorescence. The mesenchymal marker (N-cadherin) was increased significantly compared with the epithelial marker (E-cadherin) in vaginal delivery, including the LPS-treated model and the NL model. White asterisk: fetal surface of the amnion ($n=3$), scale bar = 200 μm. (**B**) Protein levels of EMT markers in fresh AECs from various sources were measured using western blot analysis ($n=8$). (**C**) Anti-F4/80 antibody was used to assess the numbers of macrophages in uteri in CS and LPS-treated models. (**D**) Macrophages in amniotic fluid were counted by FCM. Macrophages were recruited in amniotic fluid and the uterus ($n=3$). *$P<0.05$, **$P<0.01$, ***$P<0.001$

trend. To further analyze the distinction in EMT markers in fresh AECs between ED-17 CS- and LPS-treated PROM models, E-cadherin and N-cadherin were assessed using western blot in eight pregnant mice. The results revealed that N-cadherin expression was dramatically elevated in AECs, whereas E-cadherin expression demonstrated the opposite trend (Fig. 1B and S1).

Maternal macrophages are gradually enriched in the decidua as pregnancy progresses [32]. In this study, the uterus and amniotic fluid from the CS and PROM models were analyzed for macrophage recruitment using an anti-F4/80 antibody. IHC of the uterine samples revealed that F4/80-positive cells had high scores after the LPS treatment (Fig. 1C and D). The number of F4/80-positive cells in the amniotic fluid was quantified using flow cytometry. Consistent with the IHC data, the number of F4/80-positive cells following LPS treatment was greater than that with the CS model (Fig. 1D).

EVs from the amniotic fluid of CS and LPS-treated models have distinct miRNA characteristics

The EVs were isolated from the amniotic fluid of CS- and LPS-treated PROM models and characterized using TEM, NanoSight, and western blot analyses. The EVs displayed a round morphology ranging from 50 to 200 nm, tested positive for markers CD63, CD9, Tsg101, and Alix, and negative for Calnexin (Fig. 2A–C and S2). Subsequently, the miRNA profile of these EVs was analyzed; sixty-four significantly altered miRNAs were identified. The top ten miRNAs, including miR-155-5p, miR-146a-5p, miR-200c, miR-144-3p, miR-142a-3p, miR-200b, miR-Let-7i-5p, miR-181b-5p, miR-322-5p, and miR-192-5p, were transfected into AECs. The results demonstrated a significant decrease in E-cadherin levels ($p<0.01$) after ectopic expression of miR-146a-5p and miR-155-5p (Figure S3). MiR-146a-5p (miR-146a) and miR-155-5p (miR-155) are known to regulate innate immune responses and inflammation. Alterations in their expression are linked to the pathogenesis of inflammatory diseases and may trigger EMT in cancer cells [2, 33–36]. In this study, EV-miR-146a and EV-miR-155 were upregulated after LPS treatment, as evidenced by real-time PCR (Fig. 2D). It was further investigated whether EVs carrying miR-146a and miR-155 could be transferred into AECs. After treating the EVs with Triton X-100 or RNase, significant changes in miR-146a and miR-155 levels were observed, indicating effective miRNA transfer (Fig. 2E).

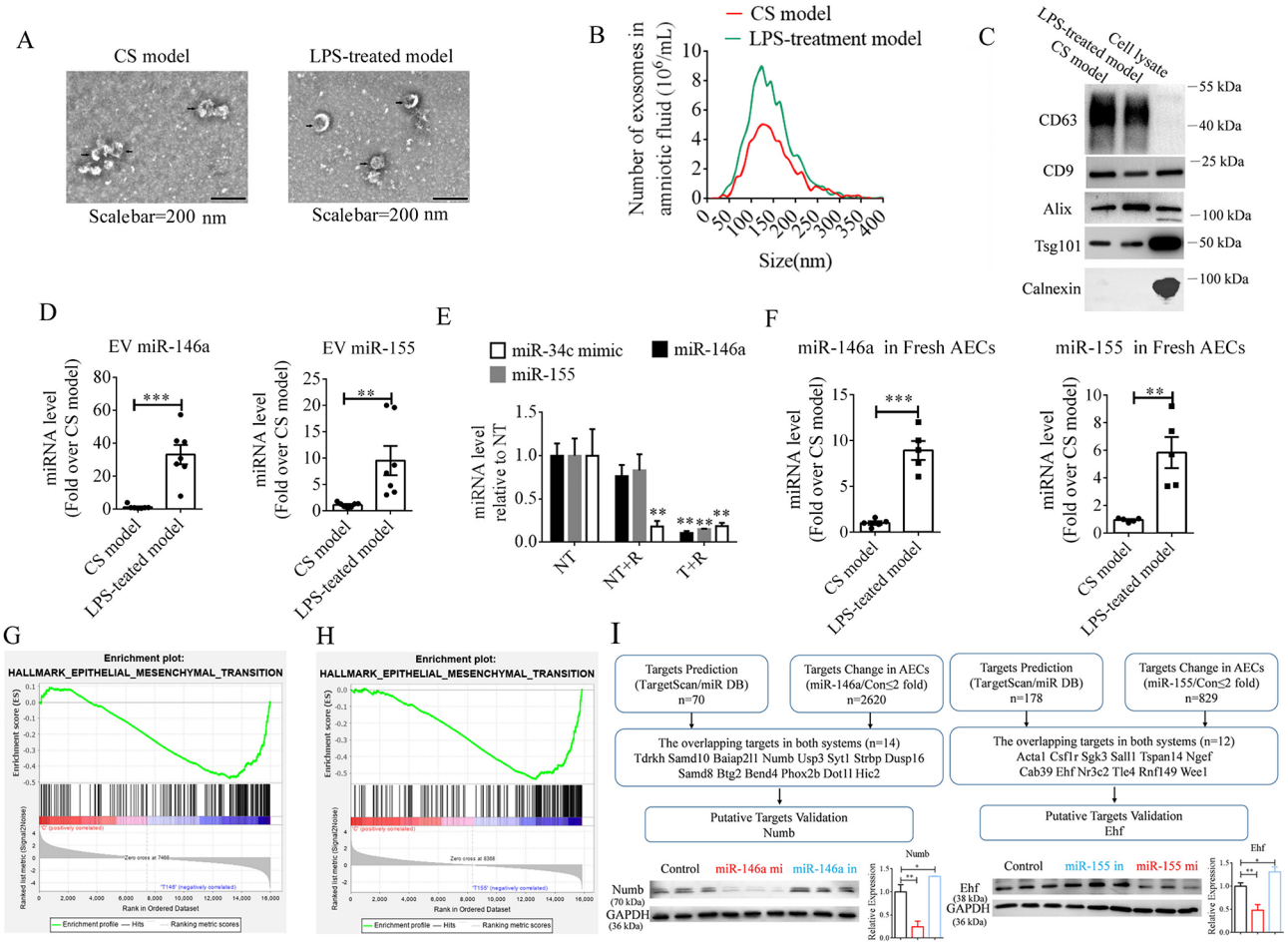

Fig. 2 Characterization of EVs from the amniotic fluid of the CS and LPS-treated models. (**A**) Visualization of EVs from the amniotic fluid by transmission electron microscopy. (**B**) Analysis of the size distribution of EVs from amniotic fluid using NanoSight technology. (**C**) Analysis of EV positive markers CD63, CD9, Tsg101, and Alix, and the negative marker Calnexine by western blot. Cell lysate, total protein from amniotic fluid-derived cells. (**D**) The abundance of miR-146a and miR-155 in EVs from the amniotic fluid of CS and LPS-treated PROM models was measured by qPCR and expressed as the fold change versus the CS model. (**E**) Levels of specific miRNAs in EVs from the amniotic fluid of LPS-treated models. MiR-34c mimic was used as a positive control for RNase digestion and spiked in the EV preparation. Samples treated with (T) or without (NT) Triton X-100 were incubated with RNase (R) and then miRNA levels were measured by qPCR and expressed as a percentage of NT ($n=3$). (**F**) MiR-146a and miR-155 abundances in fresh AECs were measured using qPCR and expressed as the fold change versus the CS model. **G** and **H**. After performing GSEA analysis on AECs overexpressing miR-146a and miR-155 respectively, significant differences in the expression of EMT-related signaling pathways were observed. The results indicated that miR-146a and miR-155 could promote the EMT process in AECs. **I**. Schematic representation for target identification of miR-146a (left panel) and miR-155 (right panel). Putative targets were obtained by overlapping differentially expressed miRNAs in AECs versus the control cells and software-predicted targets. EMT-associated target genes are shown. Western blot analysis of proteins expressed by gene targets of miR-146a and miR-155 following miRNA overexpression or knock-down in AECs. Protein abundance was analyzed using ImageJ tools. Overexpression of miR-146a/miR-155 mimics (mi) or inhibitors (in) for 72 h inhibited endogenous expression of Numb and Ehf; GAPDH was used as an endogenous control. $^*P<0.05$, $^{**}P<0.01$, $^{***}P<0.001$

EV-miRNAs from the LPS-treated model are crucial EMT triggers in AECs

The levels of miR-146a and miR-155 were initially measured in native AECs from LPS-treated pregnant mice. Fresh AECs were isolated from the amniotic tissues of CS- and LPS-treated PROM models using trypsin digestion. Real-time PCR was then performed to analyze the expression levels of miR-146a and miR-155. The miR-146a and miR-155 levels were found to be dramatically elevated in native AECs after LPS treatment (Fig. 2F). To assess potential induction of EMT in AECs by miR-146a and miR-155, overexpression of each microRNA was conducted in AECs, followed by RNA-seq analysis to detect changes in gene expression profiles. The resulting differential gene expression data were compiled in Table S1 and subjected to gene set enrichment analysis (GSEA). This analysis revealed significant changes in the epithelial-mesenchymal-transition pathway (Fig. 2G and H). To identify the targets of miR-146a and miR-155 responsible for triggering EMT, we analyzed genes that were both predicted targets of these miRNAs using TargetScan (https://www.targetscan.org/vert_80/) and miRDB (https://

mirdb.org/cgi-bin/mining.cgi) and were downregulated in AECs overexpressing the miRNAs. Fourteen putative target genes for miR-146a and twelve for miR-155 were identified. These genes are known to regulate the β-catenin pathway and molecules associated with the epithelial phenotype, such as Numb [2, 37] and Ehf [38, 39], and were also influenced by the ectopic miRNAs (Fig. 2I and S4).

Dual-luciferase reporter system analysis confirmed the interaction between miR-146a and the 3'UTR of Numb (Figure S5A). The Wnt/β-catenin signaling pathway, known to be involved in EMT and to activate Snail, was subsequently examined. Analysis of the putative target gene Numb showed reduced expression levels following miR-146a overexpression compared with the control and after miR-146a knockdown in AECs (Fig. 2I). Furthermore, GSEA revealed significant alterations in the Wnt/β-catenin signaling pathway (Figure S5B). Given that Numb regulates the stability of β-catenin through proteasome- and lysosome-dependent pathways [2], mesenchymal transited AECs were treated with the proteasome inhibitor MG132 or the lysosome inhibitor bafilomycin A1 (Baf A1). The results showed that only MG132 suppressed Numb-induced β-catenin degradation, and ectopic Numb expression increased polyubiquitylated β-catenin, suggesting that Numb promotes β-catenin polyubiquitylation (Figures S5 C, D, and S6). These findings suggest that miR-146a promotes EMT through the activation of β-catenin in AECs. Furthermore, we demonstrated the interaction between miR-155 and Ehf (Figure S7A). To further elucidate the relationship between Ehf and EMT in AECs, the promoter region of E-cadherin was cloned and used to construct a luciferase reporter system. The results clearly demonstrate that Ehf enhanced luciferase activity through interacting with the promoter region of E-cadherin (Figure S7B), indicating that miR-155 promotes EMT by inhibiting E-cadherin expression.

To confirm the regulatory interaction between miRNAs and their targets, we initially co-transfected the miR-146, miR-155, and their respective targets (Numb and Ehf) into AECs. We then assessed their functional antagonism using western blot analysis. The results, depicted in Figures S7C and S8A, showed no notable alteration in protein expression levels in AECs nor were there significant changes observed in EMT-related proteins. Further examination of the roles of miR-146a, miR-155, and their EMT targets in AECs involved the use of small interfering RNAs (siRNAs) against Numb and Ehf (si-Numb and si-Ehf, respectively), as well as the overexpressed Numb (o-Numb) and Ehf (o-Ehf). MiR-146a mimics, MiR-155 mimics, si-Numb, si-Ehf, o-Numb, and o-Ehf were all then applied to AECs either alone or in combination. The effects on AEC EMT are shown in Fig. 3A, S7D, and S8B. Single expression of si-Numb, si-Ehf, and treatments with o-Numb or o-Ehf demonstrated that si-Numb and si-Ehf promoted EMT, whereas the combination of o-Numb and o-Ehf prevented EMT and inhibited the activation of β-catenin.

MMP-9 plays a major role in the rupture of fetal membranes and is secreted by AECs after treatment with inflammatory factors [40]. In our study, the positivity rate of MMP-9 in the LPS-treated and NL models was markedly greater than that in the CS model (Fig. 3B). We also investigated the potential correlation between the Wnt/β-catenin pathway and the expression of MMP-9. Utilizing ALGGEN-PROMO (version 8.3) [41] and JASPAR (version 7) [42], the analysis showed that the transcription factor TCF7, known for its binding affinity with β-catenin, had binding sites on the EMT key gene Snail as well as the promoter region of MMP-9 (Figures S9A, B, C, and D). Using a dual-luciferase promoter reporter system, we demonstrated TCF7's ability to enhance the transcriptional activity of both MMP-9 and Snail (Figures S9E and F). The miR-146a mimics, miR-155 mimics, si-Numb, si-Ehf, o-Numb, and o-Ehf were then utilized as experimental tools to investigate MMP-9 expression in AECs. The results indicated a positive correlation between MMP-9 expression and β-catenin activation (Fig. 3C and S10).

Although the exogenous miR-146a and miR-155 derived from inflammatory EVs were finite, EMT occurred serially, indicating an induction of endogenous miR-146a and miR-155 expression. We analyzed TCF7 within the 2 kbp upstream region of pre-miR-146 and pre-miR-155. The results identified binding sites upstream of pre-miR-146 and pre-miR-155 (Figures S11 A, B, C, and D), and these interactions were further analyzed using a luciferase reporter assay. Similar to Snail and MMP-9, a physical association of Tcf7 with the miR-146a and miR-155 promoters was confirmed (Figure S11 E and F). These findings demonstrated that exogenetic miRNAs can increase the transcription of endogenous miRNAs through the Wnt /β-catenin pathway, thereby promoting EMT in AECs.

EVs from the M1 polarized macrophage promote EMT in AECs

Macrophages were identified in the decidua and amniotic fluid after LPS treatment, leading to the hypothesis that EVs from M1 polarized macrophages (M1 macrophages) play an important role in inducing EMT in AECs. Initially, macrophages were isolated from the amniotic fluid of the CS model in pregnant mice using positive magnetic isolation with an F4/80 antibody. These cells were then cultured and expanded in vitro (Figure S12 A) and designated as M0 macrophages. After stimulation by LPS and INF-γ, M0 macrophages polarize into M1 macrophages.

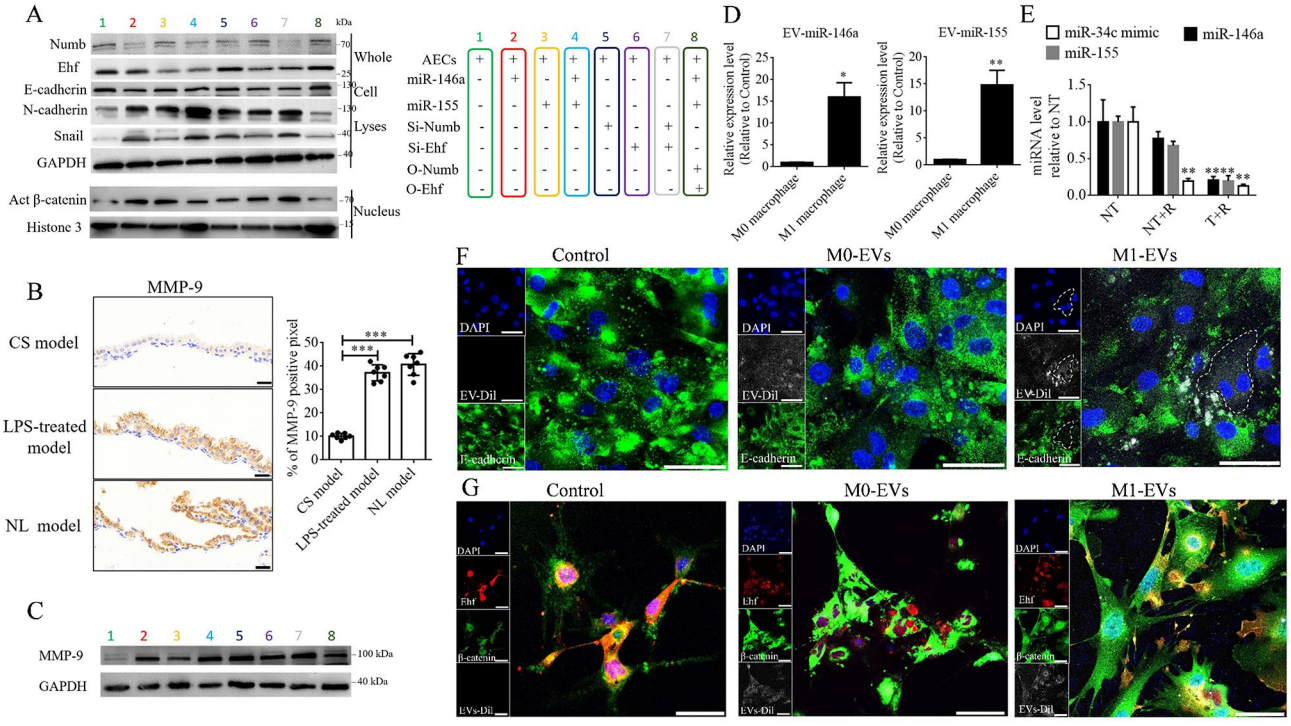

Fig. 3 Effects of EV-miRNAs and their targets on EMT and MMP-9 expression in AECs. (**A**) Western blot analysis showing that miR-155 promotes epithelial-to-mesenchymal transition in AECs by inhibiting E-cadherin expression, while miR-146a promotes EMT in AECs by activating the Wnt/β-catenin signaling pathway. (**B**) MMP-9 expression was detected by IHC in the amniotic membranes of the CS, LPS-tread, and NL models. MMP-9 increased significantly in the LPS-treated and NL models compared with the CS model. Scale bar = 100 μm. (**C**) MMP-9 expression in AECs after treatment with different elements. The results indicate that MMP-9 expression is positively correlated with the activation of the Wnt/β-catenin pathway in AECs. Quantifications of these proteins are shown in Figure S7D; data were normalized to GAPDH and relative to normal AECs ($n = 3$). Representative Western blots from three independent experiments show effects of siRNA targeting Numb (Si-Numb), siRNA targeting Ehf (Si-Ehf), overexpression of Numb (O-Numb), and overexpression of Ehf (O-Ehf). (**D**) The abundance of miR-146a and miR-155 in EVs from M0 and M1 macrophages was measured using qPCR and expressed as the fold change relative to the M0 macrophages. (**E**) Levels of specific miRNAs in EVs from M1 macrophages. A MiR-34c mimic was used as a positive control for RNase digestion and added to the EV preparation. Samples treated with (T) or without (NT) Triton X-100 were incubated with RNase (R), and then miRNA levels were quantified using qPCR and expressed as a percentage of NT ($n = 3$). (**F**) The 1×10^8 particles/mL EVs derived from M0 macrophages (M0-EVs) and M1 macrophages (M1-EVs) were incubated with AECs to analyze the expression of E-cadherin. The results indicated that the level of E-cadherin was significantly reduced in AECs after M1-EV incubation. Scale bar = 50 μm. (**G**) The immunofluorescence indicated β-catenin activation and Ehf reduction in the nucleus of AECs after M1-EV incubation. Scale bar = 50 μm. $^*P < 0.05$, $^{**}P < 0.01$, $^{***}P < 0.001$

The biogenesis of EVs starts in the endosomal system and is followed by maturation into multivesicular body (MVB), followed by MVB fusion with the plasma membrane for release outside the cells. This involves a series of genes, including Hrs, Tsg101, Stam1, Vps4B, CD9, CD63, nsMase2, Pld2, Rab11a, Rab35, Rab2b, Rab5a, Rab9a, Rab27a, Rab27b, Rab7, Ykt6, Pkm2, and Atg7 [43, 44]. Therefore, the mRNA levels of these genes in M0 and M1 macrophages were measured using real-time PCR analysis, and the results suggested that LPS and INF-γ promoted the biogenesis of EVs by upregulating the expression of Tsg101, CD63, and nsMase2, and accelerating the transport and release of EVs by increasing the expression of Rab35, Rab5a, Rab9a, Rab27a, and Rab7 (Figure S12 B). The EVs were then extracted from the M0 and M1 macrophage cellular supernatant to enable an analysis of their distinctive attributes. Notably, the morphology, sizes, and specific protein compositions of the EVs derived from the macrophages before and after LPS and INF-γ treatments exhibited no discernible alterations (Figure S12 C, D, E and Figure S13). And then the miRNA levels in the EVs derived from the macrophages were then detected, revealing that EV-miR-146a and EV-miR-155 were upregulated after LPS and INF-γ treatments (Fig. 3C). It was then determined if the EVs carrying miR-146a and miR-155 were derived from M1 macrophages. EVs were treated with Triton X-100 or RNase, and miR-146a and miR-155 levels were quantified, revealing significant changes with the different treatments (Fig. 3D).

To examine the impacts of M1-EVs on EMTs in AECs, an incubation experiment was conducted in which AECs were exposed to M1-EVs labeled with Dil at varying concentrations to determine the optimal concentration. Subsequently, a progressive increase in gray fluorescence within the AECs as the concentration of EVs increased

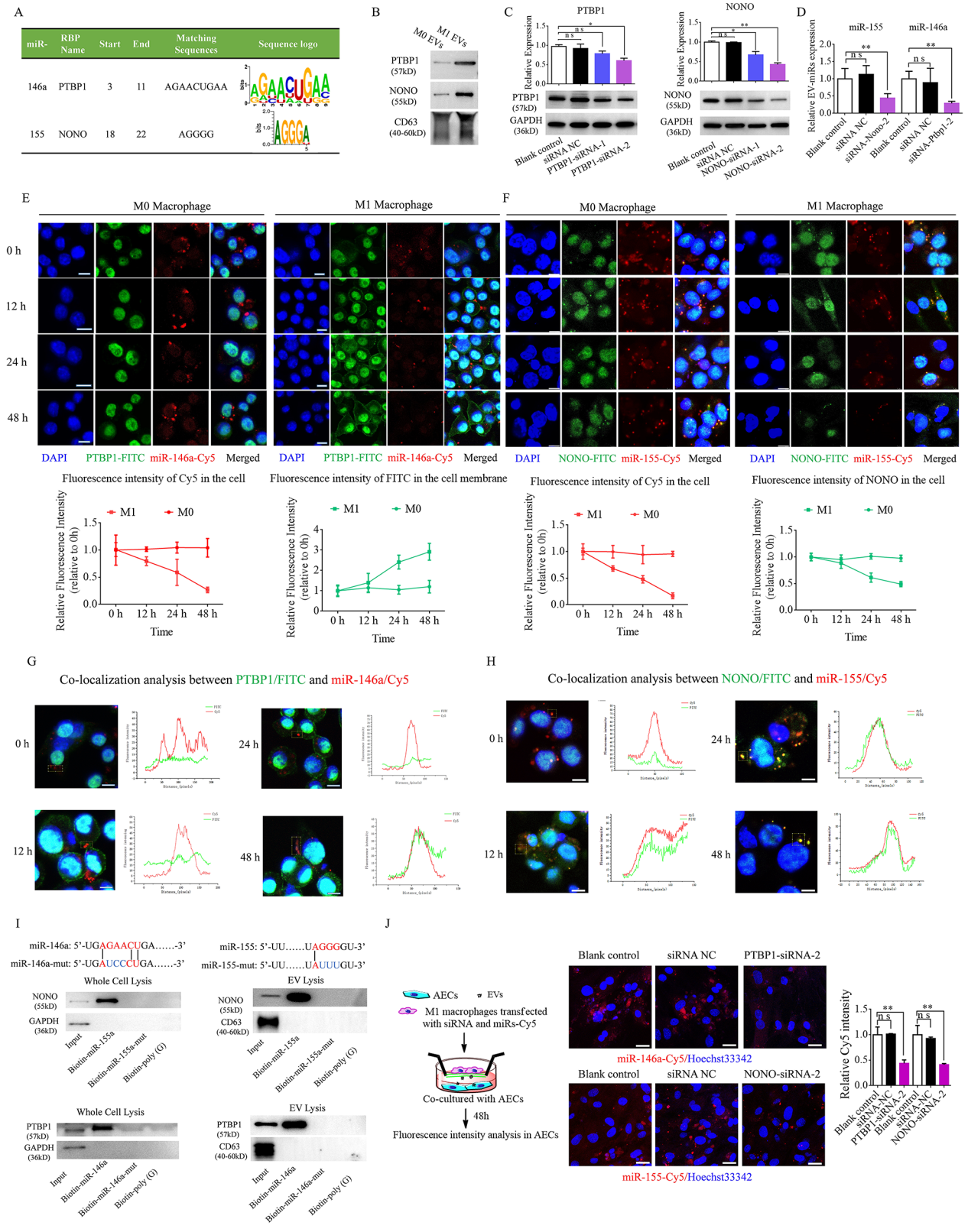

Fig. 4 (See legend on next page.)

(See figure on previous page.)

Fig. 4 RNA-binding proteins (RBPs) mediate miR-146a/155 packaging into macrophage-derived EVs. (**A**) Direct interactions between the miR-146a/155 sequences and RBP motifs were predicted using RBPDB analysis (threshold 0.5). (**B**) Western blot results showing RBP (PTBP1 and NONO) expression in macrophage-derived EVs. **C** and **D**. Western blot and qPCR results showing PTBP1 and NONO expression levels in macrophages 48 h after transfection with specific siRNAs. **E**. The levels of FITC-labeled PTBP1 and cy5-labeled miR-146a exhibit alterations throughout the polarization process of M1 macrophages. PTBP1, an RNA-binding protein for miR-146a, exhibited a shift in its expression pattern from nuclear localization to clustering on the cell membrane upon macrophage polarization. The fluorescence signal emitted by cy5 exhibits a gradual decline as the macrophage undergoes polarization within the cellular environment. **F**. Levels of FITC-labeled NONO and cy5-labeled miR-155 exhibit alterations throughout the polarization process of M1 macrophages. NONO, an RNA-binding proteins for miR-155, and miR-155 exhibit a gradual decline as the macrophage undergoes M1 polarization within the cellular environment. **G**. Co-localization analysis of PTBP1 and miR-146a reveals a gradual strengthening of the co-localization signal as macrophages polarize towards the M1 phenotype. **H**. Co-localization analysis of NONO and miR-155 reveals a gradual strengthening of the co-localization signal as macrophages polarize towards the M1 phenotype. **I**. Western blot analysis of PTBP1 and NONO expression in samples derived by biotinylated miR-146a/155 pulldowns performed with whole cell lysis, or EV lysis of macrophages, and the indicated biotinylated miR-146a/155 or mutated miR-146a/155. biotinylated poly (G) was used as a negative control. **J**. AECs were co-cultured with macrophages concurrently transfected with Cy5-miR-146a/155 and specific siRNAs targeting PTBP1 or NONO for 48 h. Fluorescence microscopy was used to detect red fluorescence signals in AECs (scale bar = 100 μm). ns, not significant, $^{*}P < 0.05$, $^{**}P < 0.01$

was observed, and it peaked from 1×10^8 to 1×10^9 particles/mL. For subsequent experiments, 1×10^8 particles/mL for the EVs was used (Figure S14). To examine the impact of M0-EVs and M1-EVs on the epithelial phenotype of AECs, the AECs were incubated separately with M0-EVs (1×10^8 particles/mL) and M1-EVs (1×10^8 particles/mL). Immunofluorescence analysis was performed to evaluate E-cadherin expression. The results revealed a significant reduction in E-cadherin expression induced by M1-EVs (Fig. 3E). Further analysis was conducted using immunofluorescence to examine the changes in β-catenin and Ehf expression in the AECs exposed to the EV treatment. Upon incubation with M1-EVs, β-catenin exhibited activation and translocation to the nucleus, while conversely, the fluorescence intensity of EHF in the nucleus decreased (Fig. 3F).

MiRNAs packaging in EVs is mediated by RNA-binding protein

Based on the levels of miR-146a and miR-155 in the EVs, it was hypothesized that macrophages package the miR-146a and miR-155 alongside specific RNA-binding proteins (RBP) into MVB and then release them outside the cells. To investigate whether miR-146a and miR-155 were specifically packaged into the EVs, the specific interactions between the miR-146a and miR-155 sequences and the motifs for the RNA-binding proteins were analyzed using a database for RNA-binding specificity (http://rbpdb.ccbr.utoronto.ca/; threshold 0.5) [45]. The results indicate that the polypyrimidine tract-binding protein 1 (PTBP1) motif exhibited a specific binding site for miR-146a, whereas the non-POU domain-containing octamer-binding protein (NONO) motif exhibited a specific binding site for miR-155 (Fig. 4A). Western blot was performed to confirm the presence of PTBP1 and NONO in macrophage-derived EVs (Fig. 4B and Figure S15). Subsequent experiments revealed that the use of specific siRNAs to suppress PTBP1 and NONO in M1 macrophages resulted in substantial reductions in the quantities of EV-miR-146a and EV-miR-155 (Fig. 4C, Figure S16, and Fig. 4D). This indicates that PTBP1 and NONO are involved in the regulation of EV-miR-146a and EV-miR-155 levels. To enhance the visualization of the analysis pertaining to the extracellular transportation of miRNAs by RBPs, cy5-labeled miRNAs were introduced into M0 macrophages via transfection. Subsequently, immunofluorescence analysis was conducted to assess alterations in the expression of miRNAs and RBPs prior to and following M1 macrophage polarization. These findings indicate that the binding protein PTBP1 associated with miR-146a exhibited a shift in its expression pattern from nuclear localization to clustering on the cell membrane with M1 macrophage polarization. Meanwhile, the binding protein NONO linked to miR-155 showed a transition from nuclear localization to distribution throughout the cell, and this was accompanied by a reduction in its expression levels (Fig. 4E and F). Fluorescence co-localization analysis revealed that with the elongation of polarization for M1 macrophages, the red fluorescence emitted by Cy5-labeled miRNAs and the green fluorescence emitted by FITC-labeled RBPs progressively converged at identical pixel positions. This indicated that the interaction between these two entities occurred after M1 macrophage polarization (Fig. 4G and H). Moreover, miRNA pull-down assays showed an interaction between RBPs and miRNAs in whole-cell and EV lysis. However, RBP-binding capacity was impaired when the combined site sequences of the miRNAs were mutated (Fig. 4I and Figure S17). Functionally, confocal analysis demonstrated a reduction in the transfer of miRNAs from M1 macrophages to AECs via EVs when the macrophages were pre-transfected with PTBP1- or NONO-specific siRNAs (Fig. 4J).

Changes in the EV-miRNAs in M1 macrophages after different treatments influenced EMTs in AECs, bothin vivo and in vitro

To validate the transportation of PTBP1/NONO-bound miR-146a/155 to EVs in M1 macrophages, as well as the uptake of miR-146a/155-carrying EVs by AECs, and

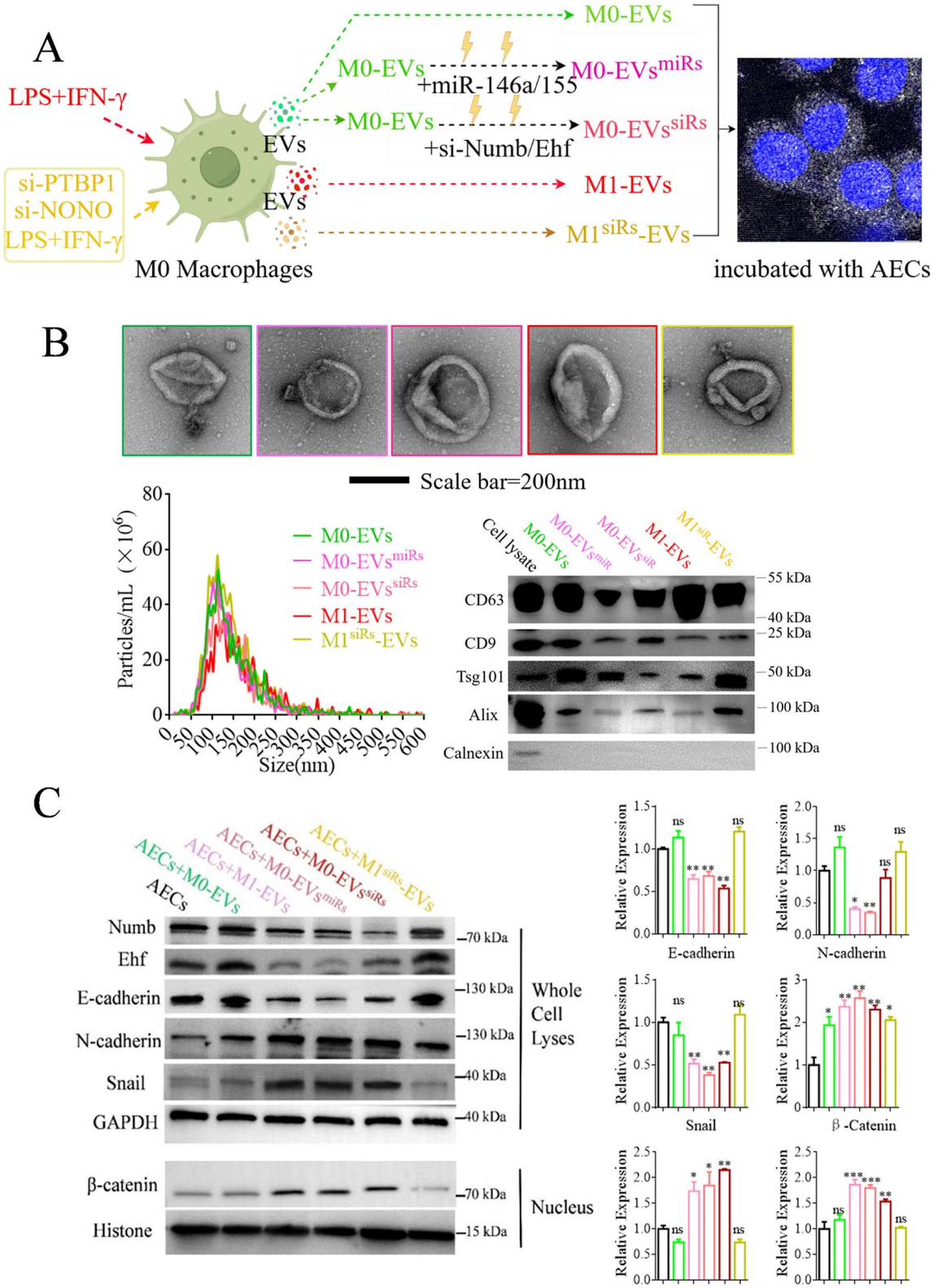

Fig. 5 (See legend on next page.)

(See figure on previous page.)

Fig. 5 Role of EVs derived from macrophages after different treatments during EMTs in AECs in vitro. (**A**) Diagram showing the different treatments in macrophages, or EVs, and the obtained M0-EVs, M0-EVs^{miRs}, M0-EVs^{siRs}, M1-EVs, and M1^{siRs}-EVs. (**B**) Biological characteristics of these EVs, including morphology, particulate size distribution, and EV marker proteins. (**C**) Expression of EMT key genes and β-catenin expression in AECs after incubation with different EVs. The results indicate that Numb, Ehf, and E-cadherin were dramatically reduced, and the activation of β-catenin in AECs after incubation with M0-EVs^{miRs}, M0-EVs^{siRs} and M1-EVs. Conversely, opposite data were observed in M0-EVs and M1^{siRs}-EVs. Quantification of these proteins is shown in the right panel, data were normalized to GAPDH and relative to AECs ($n = 3$). Representative blots from three independent experiments are shown. ns, not significant, $^{*}P < 0.05$, $^{**}P < 0.01$, $^{***}P < 0.001$

the impact of miR-146a/155 on target genes Numb/Ehf to facilitate EMT, miR-146a/155 or si-Numb/Ehf was loaded into EVs derived from M0 macrophages (named M0-EVs^{miRs} and M0-EVs^{siRs}). The EVs were then collected after interfering with PTBP1 and NONO expression in M1 macrophages (named M1^{siRs}-EVs). A schematic illustration of the process is shown in Fig. 5A, and the effects of the modified EVs on promoting the EMT of AECs were compared, respectively. Subsequently, the morphology, size, and characteristic EV marker proteins of the M0-EVs, M0-EVs^{miRs}, M0-EVs^{siRs} M1-EVs, and M1^{siRs}-EVs were analyzed (Fig. 5B and Figure S18). Transmission electron microscopy (TEM) analysis showed that the EVs exhibited spherical morphologies and were structurally intact without membrane impairment. Nanoparticle tracking analysis (NTA) revealed that the average diameters of the M0-EVs, M0-EVs^{miRs}, M0-EVs^{siRs} M1-EVs, and M1^{siRs}-EVs were comparable and fell within the established size range for EVs (50–200 nm). Immunoblotting results indicated the presence of characteristic EV marker proteins, namely, CD63, CD9, Alix, and Tsg101, whereas calnxin was absent in all EV samples. The AECs were then exposed to these EVs for 48 h, and immunoblotting was used to analyze for EMTs and the activation of the Wnt/β-catenin pathway. M1-EVs and M0-EVs loaded with miR-146a/155 or si-Numb/Ehf, effectively facilitated EMTs in AECs and induced activation of the Wnt/β-catenin pathway within 48 h. In contrast, the M0-EVs and M1^{siRs}-EVs were ineffective (Fig. 5C and Figure S19).

The potential of the M1-EVs to induce EMTs in AECs and trigger PROM in vivo was then investigated. To achieve this, M1-EVs at varying concentrations were labeled with DiR and delivered to pregnant mice via intrauterine injection. After 12 h, the distribution of DiR-labeled M1-EVs was analyzed using whole-body and organ fluorescence. The DiR fluorescence was predominantly localized in the abdominal region and exhibited a positive correlation with the M1-EV concentration (Fig. 6A). Subsequent fluorescence analysis of multiple organs revealed the presence of fluorescence in the uterus, fetal membranes, liver, and kidneys, indicating that the M1-EVs have the ability to traverse the maternal-fetal barrier and undergo metabolic processes within the maternal organism. Examination of the timing of PROM revealed a positive correlation between the concentration of M1-EVs and the duration of their occurrence. Specifically, an increase in the M1-EV concentration led to a gradual reduction in the duration of PROM. Notably, the duration of PROM induced by 1×10^6 particles per head of M1-EVs was similar to that caused by the LPS treatment, whereas the shortest duration was observed in cases involving 1×10^8 particles per head (Fig. 6B). Further investigations were performed to examine the distribution of M1-EVs in the amnion. Dil-labeled M1-EVs were administered via intrauterine injection, the amnion was collected for preparing frozen sections, and the fluorescence intensity of the Dil was observed. Additionally, immunofluorescence analysis was performed to assess the expression of E-cadherin and N-cadherin (Fig. 6C and D). Notably, an increase in the fluorescence intensity of Dil corresponded to a gradual increase in the expression of N-cadherin and a decrease in the expression level of E-cadherin. These findings suggest that M1-EVs influence the EMTs in AECs, thereby modulating the incidence of PROM.

M0-EVs, M0-EVs^{miRs}, M0-EVs^{siRs}, M1-EVs, and M1^{siRs}-EVs, each at a concentration of 1×10^8 particles per head, were used to investigate the impact of these EVs on PROM. A comprehensive examination of whole-body fluorescence revealed that the fluorescence signal from the EVs was predominantly localized in the abdomen, indicating that EV modification did not alter the distribution patterns (Fig. 7A). Evaluations of the timing of PROM incidence showed that M0-EVs exerted no significant influence on PROM, whereas the loading of miRNAs or siRNAs into EVs promoted PROM. Interference of PTBP-1/NONO expression with siRNA in M1 macrophages significantly altered the timing of PROM occurrence, facilitated by M1-EVs. These findings suggest the crucial involvement of miR-146a/155 in M1-EVs during PROM (Fig. 7B). Immunofluorescence analysis was also performed to determine E-cadherin and N-cadherin expression levels in the amnion. The results revealed no significant difference in the levels of E-cadherin between the CS-control and M0-EV treatment groups. However, the level of N-cadherin was substantially increased in both the M1-EVs and M0-EVsmiRs groups (Fig. 7C and D).

Subsequently, western blot analysis was employed to assess the expression levels of miRNA target genes (Numb and Ehf), key EMT genes (E-cadherin, N-cadherin, and Snail), and MMP-9 in amniotic membranes from pregnant mice subjected to various treatments. A

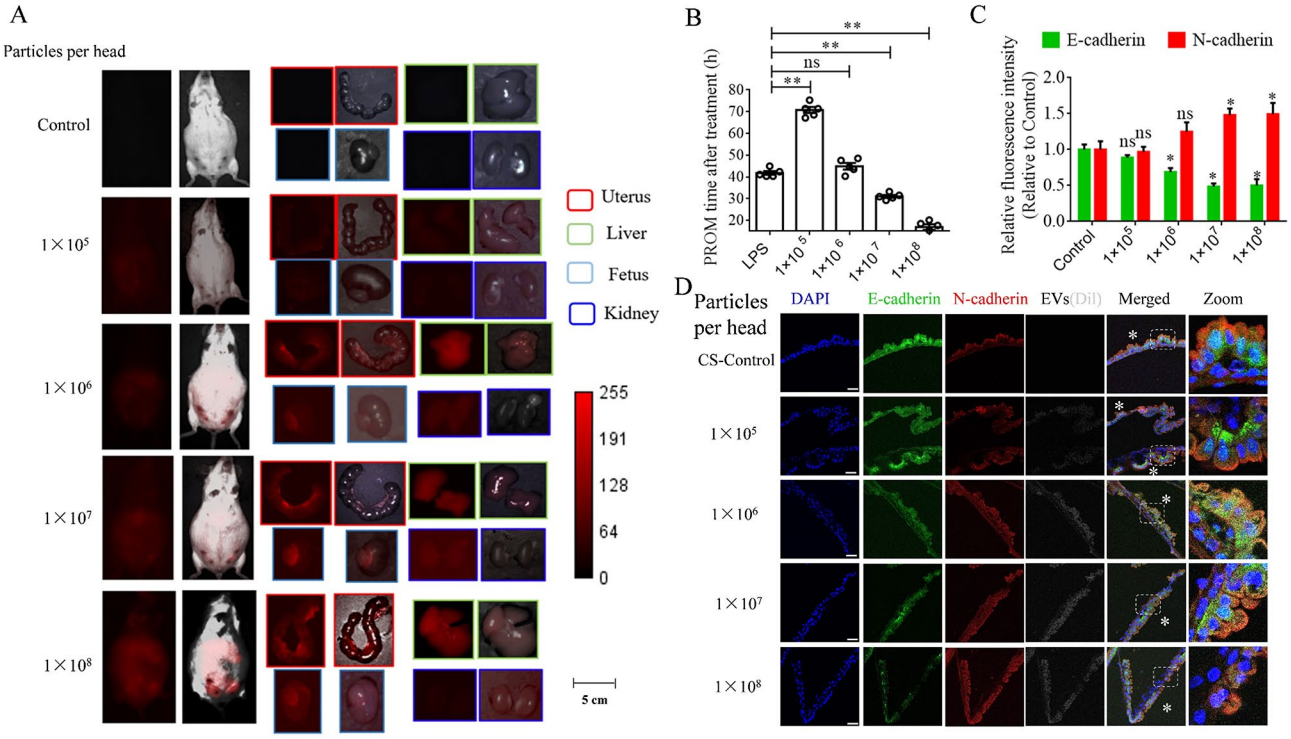

Fig. 6 Different concentrations of M1-EVs promote mouse PROM. (**A**) Representative fluorescence imaging of various M1-EVs in the whole-body and organ tissues from PROM mice. (**B**) Analysis of the PROM time after different treatments in the mouse model. **C** and **D**. The mesenchymal marker (N-cadherin) and epithelial marker (E-cadherin) for native AECs were analyzed by immunofluorescence. Mesenchymal marker (N-cadherin) increased significantly with increasing concentrations of M1-EVs, but the opposite trend was found for the epithelial marker; $N = 3$; white asterisk: fetal surface of the amnion; scale bar = 200 μm. ns, not significant, $^{*}P < 0.05$, $^{**}P < 0.01$

significant decrease in the expression of miRNA target genes and E-cadherin in the LPS-treated group, M1-EVs-treated group, M0-EVs^{siRs}-treated group, and M0-EVs-^{miRs}-treated group, compared to the CS-control group was observed. Conversely, the expression of N-cadherin, Snail, and MMP-9 was significantly upregulated in the aforementioned groups. However, it is noteworthy that the groups treated with M0-EVs and M1^{siRs}-EVs exhibited contrasting outcomes, indicating that M1-EVs facilitated EMTs in AECs through the transportation of miRNAs (Fig. 8A, Figure S20 and S21). Following EMT, epithelial cells experience a loss in their characteristic epithelial phenotype, resulting in alterations to the integrity of cell-cell junctions. We used TEM to examine modifications in cell junctions among various groups of AECs. The results indicate noteworthy transformations in the cell junctions subsequent to EMT (Fig. 8B), notably a reduction in the abundance of desmosomes and an augmentation in intercellular gaps. These alterations in the AEC cell junctions also induce corresponding modifications to the biomechanical properties of the amnion, and these were consequently assessed using force-distance (FD)-based atomic force microscopy, which measures the lowest Young's modulus of the amniotic tissue. The lowest Young's modulus values aligned with the TEM results, indicating that amniotic tissues were characterized by wider cell gaps and reduced biomechanical properties, whereas the biomechanical properties of amniotic tissues with enhanced AEC tightness were increased (Fig. 8C).

M1-EVs containing miR-146a/155 prompt EMTs in AECs and diminish the biomechanical properties of the human amnion

To determine the applicability of the theory that M1-EVs induce PROM in pregnant mice, samples of amniotic fluid (AF) and amniotic membrane (AM) from gravidas with bacterial vaginosis-induced PROM were procured from obstetric clinics. These samples were compared with the AF and AM obtained from CS gravida, which served as the normal controls (Normal-AF and Normal-AM). The initial analysis focused on assessing changes in the macrophage proportion in the AF. The results indicated that a notable increase in the proportion of macrophages in the AF induced by bacterial vaginosis in cases with PROM was observed (Fig. 9A). Subsequently, EVs were isolated from Normal-AF and PROM-AF for further biological characterization studies. These AF-EVs were in line with their known biological characteristics (Fig. 9B, C, D and Figure S22). Validation experiments were then conducted to confirm the expression of EV-miR-146a/155 in the

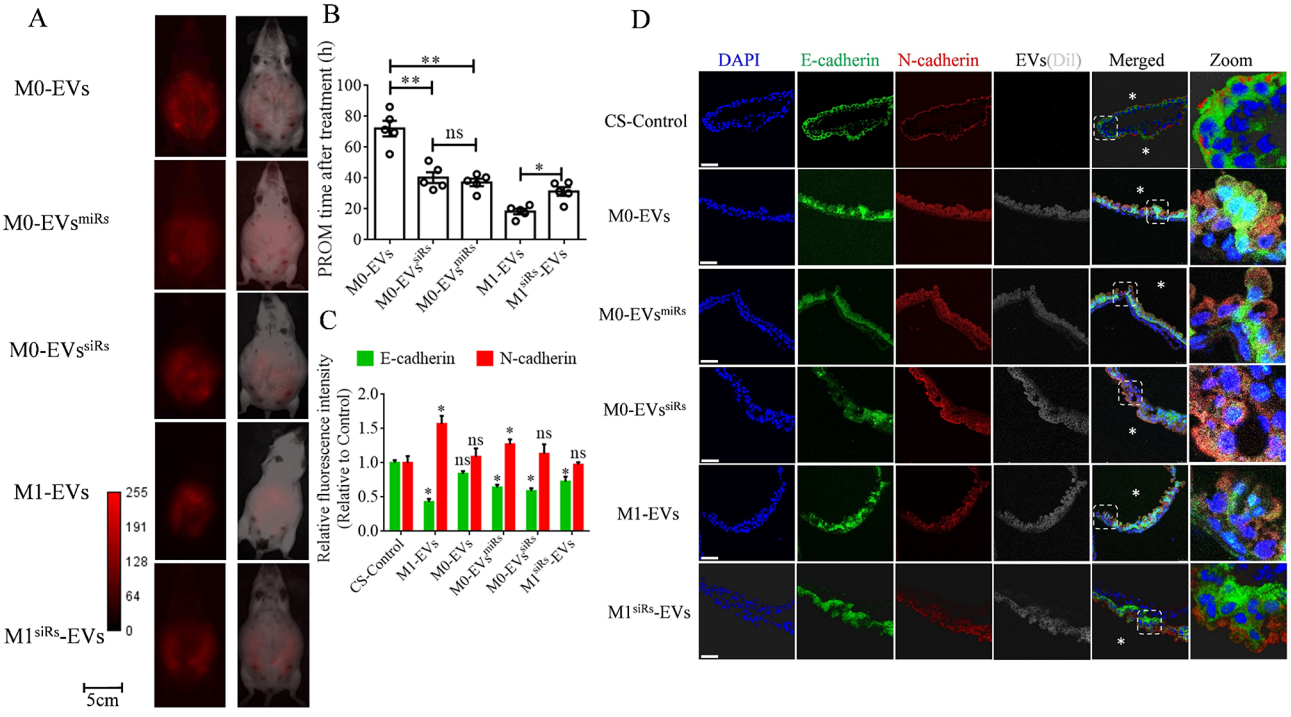

Fig. 7 Role of EVs derived from macrophages after different treatments in PROM. (**A**) Representative fluorescence imaging of various EVs in the whole-body from PROM mice. (**B**) Analysis of the PROM time after various EV treatments in the mouse model. **C** and **D**. Mesenchymal marker (N-cadherin) and epithelial marker (E-cadherin) of the native AECs were analyzed by immunofluorescence. Mesenchymal marker (N-cadherin) was increased significantly after treatment with the M0-EVs^{miRs}, M0-EVs^{siRs}, and M1-EVs, but the opposite trend was found with the epithelial marker. $N = 3$. White asterisk: fetal surface of the amnion; scale bar = 200 μm. ns, not significant, $^{*}P < 0.05$, $^{**}P < 0.01$

amniotic fluid. Real-time PCR confirmed the presence of miR-146a/155 expression in the PROM-AF-EVs (Fig. 9E), with significantly higher expression levels in PROM-AF-EVs than in Normal-AF-EVs (Fig. 9F). The expression of target genes, including miR-146a/155, NUMB/EHF, key EMT genes (ECAD, NCAD, and SNAIL), and MMP-9, was assessed in both the Normal-AM and PROM-AM samples. Western blot analysis revealed a significant reduction in the levels of NUMB, EHF, and ECAD in the PROM-AM cells, whereas the expression of EMT-related genes was upregulated (Fig. 9G, H and Figure S23). The results were further validated using immunofluorescence staining (Fig. 9I).

Subsequently, CD14-positive macrophages were extracted from the Normal-AF and cultured to obtain hM0 macrophages. Following stimulation with LPS and INF-γ, the hM0 macrophages were polarized to hM1 macrophages. The cell supernatants were then used to isolate hM0-EVs and hM1-EVs. The biological attributes of hM0-EVs, hM1-EVs, and hEV-miR-146a/155 were verified (Figure S24 and S25). The normal-AM were then incubated with 10^8 particles/mL of hM1-EVs or hM0-EVs for 48 h respectively, and western blot and immunofluorescence were used to analyze the expression of NUMB, EHF, ECAD, NCAD, SNAIL, and MMP-9. hM1-EVs reduced the expression of NUMB, EHF, and ECAD, while increasing the expression of NCAD, SNAIL, and MMP-9 (Fig. 10A, B and Figure S26). Additionally, immunofluorescence analysis of the amniotic membrane provided further evidence of the nuclear activation of β-catenin and downregulation of EHF in PROM samples, which was consistent with the observed effects of the hM1-EVs treatment on the amniotic membrane (Fig. 10C and D). Analysis of the tightness of hAECs junctions and the biomechanical properties (Young's modulus) of AM revealed results consistent with those of the mouse model. In PROM-AM, the junctions between the AECs were altered, resulting in a significant increase in intercellular gaps and a decrease in the Young's modulus of AM. When Normal-AM was treated with hM1-EVs, the junctions between cells were disrupted, leading to an increase in intercellular gaps and a decrease in the Young's modulus of AM (Fig. 10E, F, and G). In summary, this investigation employed the PROM model in mice and PROM clinical samples to elucidate the mechanism by which certain miRNAs, transported by M1-EVs, infiltrate AECs and trigger the activation of the WNT/beta-catenin pathway, while the expression of the EHF is diminished, culminating in the loss of the epithelial phenotype in AECs. This, in turn, disrupts the intercellular connections, enlarges the intercellular gaps, and impairs

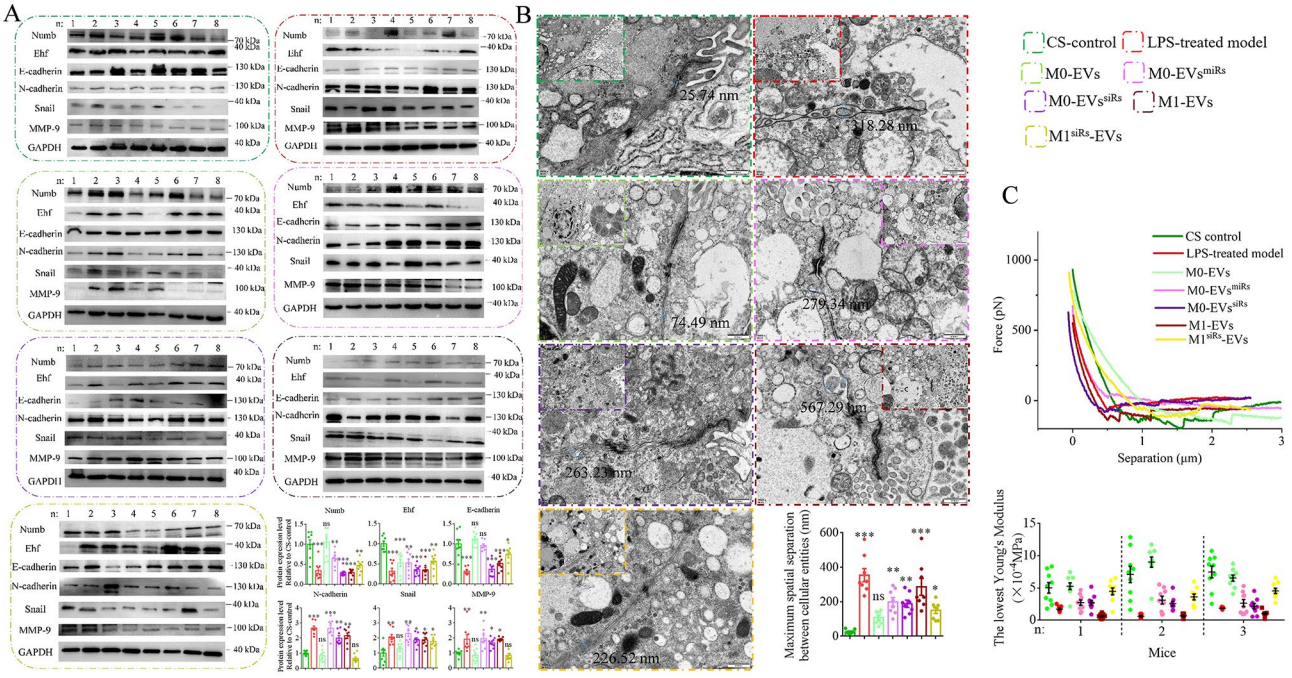

Fig. 8 Analysis of the EMT and biomechanical properties in amniotic membranes from various treated pregnant mice. (**A**) Western blot analysis of EMT key gene expression levels in the amnion after treatment with different EVs. The M0-EVs^{miRs}, M0-EVs^{siRs}, and M1-EVs facilitate the process of EMT and MMP-9 expression in the amnion, but the opposite result was observed in the M0-EVs and M1^{siRs}-EVs. (**B**) Cell junctions of the AECs were analyzed in amniotic membranes from various treated pregnant mice. The maximum spatial separation between AECs was assessed in these amniotic membranes. The data revealed that intercellular gaps between the adjacent AECs were dramatically elevated in amniotic membranes of pregnant mice treated with M0-EVs^{miRs}, M0-EVs^{siRs}, and M1-EVs. (**C**) The biomechanical properties of the amniotic membranes were analyzed via force-distance (FD)-based atomic force microscopy. Force-distance (FD) curves for the amniotic membranes of various treated pregnant mice were mapped and shown in the upper-panel. The Young's modulus values were calculated using the FD curve. An average of nine points were assessed on each amniotic membrane to determine the Young's modulus, with the lowest value for selection. A total of nine amniotic membranes were examined for each pregnant mouse. The lowest Young's modulus values are shown in the lower-panel. ns, not significant, $^{*}P < 0.05$, $^{**}P < 0.01$, $^{***}P < 0.001$

the biomechanical properties of the amnion, ultimately leading to membrane rupture (Fig. 11).

Discussion

Numerous reports have revealed the functional importance of EVs in various biological processes, such as intracellular communications [46], cell signaling [47], tissue regeneration [48], and immune responses [49]. The source of EVs in the amniotic fluid was uncertain, which are released by skin cells of the fetus, monocytes, macrophages, erythrocytes, amniotic fluid stem cells, and the placenta. Macrophages are plastic effector cells within the immune system that activate inflammation and remove pathogens and apoptotic cells. Furthermore, maternal macrophages are gradually enriched in the decidua as a result of pregnancy [32]. In this study, we observed a significant recruitment of macrophages to the amniotic fluid after LPS treatment in pregnant mice and pregnant women with reproductive tract infections. These macrophages can be roughly categorized into two functional phenotypes: the M1-type (classically activated) and the M2-type (alternatively activated). M1 macrophages are pro-inflammatory and exhibit antimicrobial properties during inflammation. The macrophages in the amniotic fluid and decidua are thus activated and transition to M1 macrophages upon LPS treatment or bacterial infection. Activated macrophages release a significant quantity of inflammatory factors, such as extracellular vesicles, which can elicit apoptosis in recipient cells by carrying special miRNAs [50, 51]. Macrophages obtained from amniotic fluids are polarized towards the M1 phenotype and subsequently release EVs containing miR-146a and miR-155. MiR-146a and miR-155 help to control innate immune responses and inflammation, and changes in their expression levels are associated with the pathogenesis of inflammatory diseases. In this study, miR-146a was found to play an important role in the activation of the Wnt/β-catenin pathway by preventing the expression of Numb. Canonical Wnt signaling is mediated by the transcriptional effector β-catenin. It has been established that in the absence of Wnt signaling, β-catenin is phosphorylated by a destruction complex that consists of GSK-3β, APC, and axin. However, little is known about Numb interactions with β-catenin degradation via the proteasome-dependent pathway. Active β-catenin enters

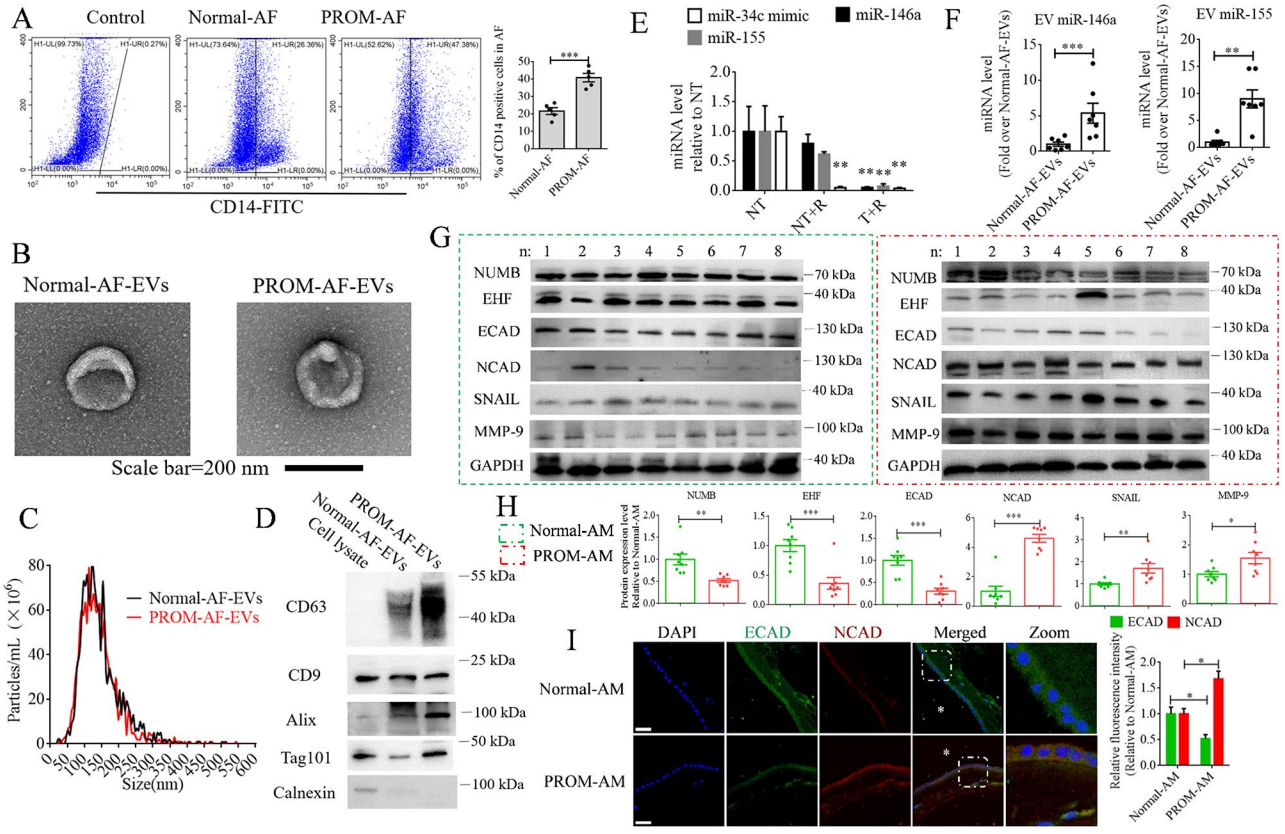

Fig. 9 Characterization of the amniotic membrane from the gravida with PROM and cesarean section (Normal). (**A**) Macrophages in the amniotic fluid from PROM and Normal were counted using FCM, and macrophages were recruited in the amniotic fluid of PROM. (**B**) Visualization of EVs from the amniotic fluid by transmission electron microscopy. (**C**) Analysis of the size distribution of the EVs from the amniotic fluid using NanoSight technology. (**D**) Analysis of the EV positive markers CD63, CD9, Tsg101, and Alix, and the negative marker Calnexine by western blot. Cell lysate, total protein from the amniotic fluid-derived cells. (**E**) Levels of specific miRNAs in the EVs from the amniotic fluid of PROM. MiR-34c mimic was used as a positive control for RNase digestion and spiked in the EV preparation. Samples treated with (T) or without (NT) Triton X-100 were incubated with RNase (R) and then miRNA levels were measured by qPCR and expressed as a percentage of NT ($n=3$). (**F**) The abundance of miR-146a and miR-155 in EVs from the amniotic fluids of the Normal and PROM were measured using qPCR and expressed as the fold change versus the Normal-AF-EVs. G and H. Western blot analysis of EMT key gene expression levels in the amnion from Normal-AM and PROM-AM; $N=8$. Epithelial-mesenchymal transition occurred in amniotic tissue derived from PROM. I. EMT key markers of native AECs were analyzed by immunofluorescence. Mesenchymal marker (N-cadherin) increased significantly in PROM-AM compared with Normal-AM, but the opposite trend was found with the epithelial marker (E-cadherin). White asterisk: fetal surface of the amnion; scale bar = 200 μm. *$P<0.05$, **$P<0.01$, ***$P<0.001$

the nucleus to accumulate and function as a co-activator for the transcription factor TCF/LEF.

Epithelial-mesenchymal transition is accompanied by specific changes in gene expression, such as the down-regulation of E-cadherin. The E-cadherin promoter is repressed by several transcriptional repressors, including the zinc finger transcription factor, Snail. Ehf is also known as an ETS homologous factor, and it plays a vital role in the differentiation and development of various epithelial tissues. It directly binds to the promoter sequence of E-cadherin, thereby enhancing its upregulation [39]. In this study, Ehf was shown to promote the transcription of E-cadherin, and the activation of M1 macrophages increased the expression of miR-155 in the EVs. MiR-155, in turn, directly inhibits the expression of Ehf, leading to the further suppression of E-cadherin expression and the promotion of EMTs in AECs.

Epithelial cells exhibit robust cell-cell adhesion facilitated by specific junctions, which serve as specialized adhesive sites where various transmembrane glycoproteins interact with the cytoskeleton. Cell–cell adhesion is primarily involved in three types of junctional complexes: tight junctions, adheren junctions, and desmosomes [52]. Despite the distinct mechanisms of formation, regulation, and function exhibited by each junction, there is significant interplay among them, which affects their dynamics and signaling properties. Early experiments involving E-cadherin inhibition suggested that its adhesion-dependent mechanism is crucial for the establishment of other specialized cell-cell junctions [53, 54]. In this study, the effects of M1-EVs on AECs were investigated. The

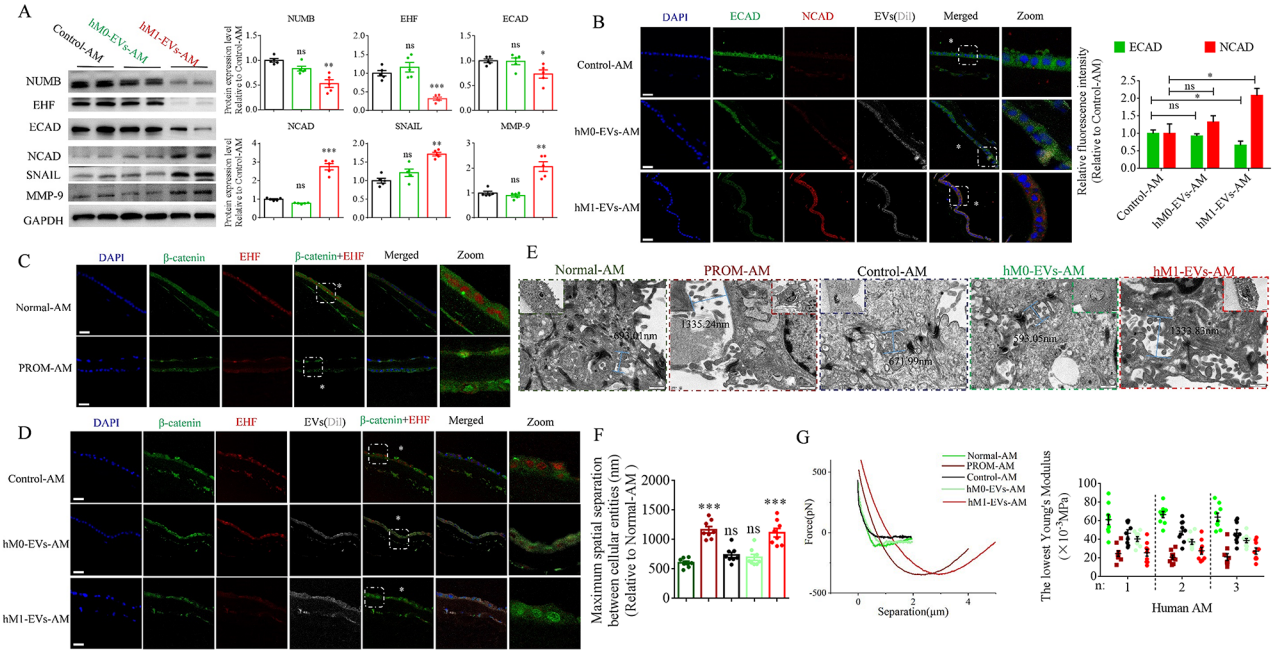

Fig. 10 Analysis of EMT and biomechanical properties in the Normal-AM of gravida after treatment by EVs derived from human macrophages. (**A**) Western blot analysis of key EMT gene expression levels in the amnion after treatment with different EVs derived from human M0 or M1 macrophages. The hM1-EVs significantly facilitate the process of EMT and MMP-9 expression in the human amnion; $n = 5$. (**B**) EMT key markers of native AECs were analyzed by immunofluorescence in PROM-AM and Normal-AM. The mesenchymal marker (NCAD) was increased significantly in the PROM-AM when compared with Nomal-AM, but the opposite trend was found with the epithelial marker (ECAD). White asterisk: fetal surface of the amnion; scale bar = 200 μm. (**C**) β-catenin activation and EHF expression were analyzed by immunofluorescence in PROM-AM and Normal-AM. In the context of Normal-AM, the expression of EHF is observed within the nuclei of the AECs, whereas β-catenin is predominantly expressed within the cytoplasm. Conversely, in PROM-AM, there is a notable decrease in EHF expression, accompanied by an accumulation of β-catenin within the nuclei. White asterisk: fetal surface of the amnion; scale bar = 200 μm. (**D**) β-catenin activation and EHF expression were analyzed by immunofluorescence in Normal-AM before and after treatment with the EVs derived from human M0 and M1 macrophages. Following treatment with hM1-EVs, the expression of EHF was diminished, while the activation and nuclear expression of β-catenin were detected. White asterisk: fetal surface of the amnion; scale bar = 200 μm. (**E**) AEC cell junctions were analyzed in human amniotic membranes with transmission electron microscopy. The representative images revealed that intercellular gaps between the adjacent AECs were dramatically elevated in amniotic membranes from the gravida with PROM and treated with EVs derived from human M1 macrophages. Scale bar = 500 nm. (**F**) Analysis of the intercellular gap size between the adjacent amniotic epithelial cells (AECs) in various treatment groups. The maximum gap value between AECs was quantified for each amniotic membrane, with a total of 8 amniotic membrane tissues included in each group for subsequent statistical analyses. The findings revealed a noteworthy elevation in the maximum gap between PROM-AM and hM1-EVs-AM, when compared to the Normal-AM group. (**G**) Biomechanical properties in human amniotic membranes were analyzed via force-distance (FD)-based atomic force microscopy. Force-distance (FD) curves for the human amniotic membranes from gravida with CS (Normal-AM), PROM (PROM-AM), and cultured Normal AM (Contorl-AM), Contorl-AM incubated with hM0-EVs (hM0-EVs-AM) or Contorl-AM incubated with hM0-EVs (Hm1-EVs-AM) were mapped and are shown in the left-panel. The Young's modulus values were calculated using the FD curve. An average of nine points were assessed for each amniotic membrane to determine the Young's modulus, with the lowest value being selected. A total of eight amniotic membranes were examined for each group. The lowest Young's modulus values are shown in the right-panel. ns, not significant, $^{*}P < 0.05$, $^{**}P < 0.01$, $^{***}P < 0.001$

resulting data revealed alterations in intercellular connections, a reduction in bridge granule quantity, and an augmentation of the intercellular gap. The observed increase in the intercellular gap in the AECs was anticipated to affect the load-bearing capacity of the amniotic membrane. Subsequently, atomic force microscopy (AFM) was used to assess the Young's modulus of both mouse and human amniotic membranes before and after treatment with M1-EVs. The utilization of AFM for indentation has emerged as a potent technique in the examination of the localized micromechanical characteristics of diverse biological tissues, cells, and biomaterials [55, 56]. Young's modulus, which gauges the rigidity or elasticity resistance of a solid when subjected to a load, can be effectively assessed using AFM. This methodology enables the spatial depiction and quantitative evaluation of the Young's modulus in relation to the amniotic tissue. The relationship between the Young's modulus of the human amniotic membrane was found to be directly proportional to that of the epithelial cells in the membrane, whereas it was inversely proportional to the stromal cells. Benson-Martin et al. conducted an experiment using a stress-strain apparatus to determine the Young's modulus of both normal amniotic membranes and membranes with premature rupture [57]. However, one limitation of this study is the inability to accurately replicate the forces exerted by the fetus on the amniotic membrane in vivo. In another study, the mechanical properties of the fetal

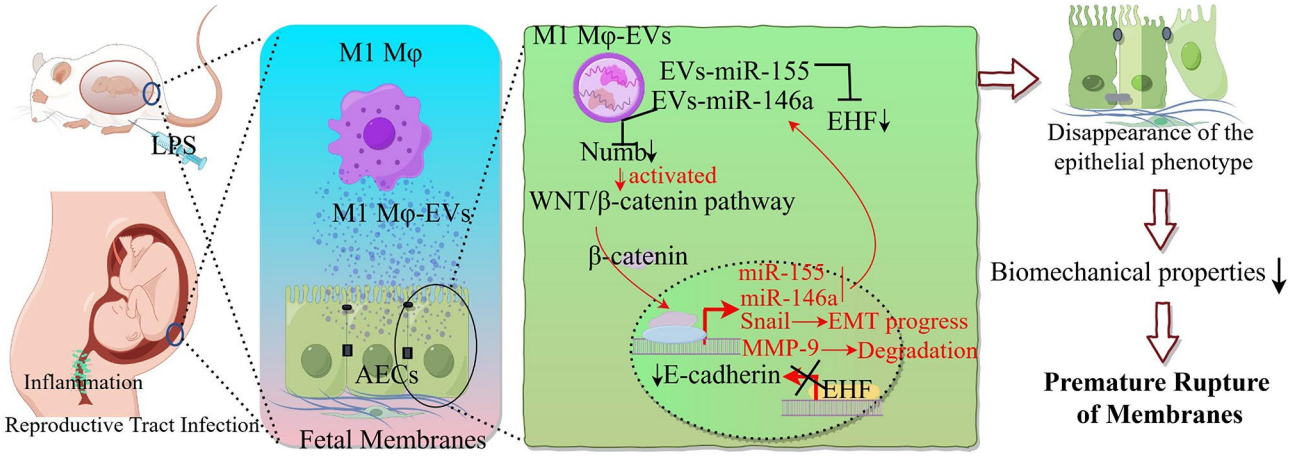

Fig. 11 Schematic diagram depicting the mechanism through which M1-EVs induce EMTs in AECs, subsequently triggering preterm premature rupture of membranes in both mice and humans

membranes in both preterm and term samples, were assessed using ball indentation and optical coherence elastography techniques [58]. Overall, the non-ruptured site exhibited higher stiffness than the ruptured site. In this study, AFM was used to quantify the lowest Young's moduli of human and murine amniotic membranes. These results were consistent with those from the cell adhesion detection. Notably, the transition of amniotic epithelial cells from an epithelial to a mesenchymal state reduced the lowest Young's moduli in the amniotic membrane tissue.

Conclusions

In this study, EV-miR-146a/155 from M1 macrophages were found to trigger EMTs and MMP-9 transcription in AECs under inflammatory conditions. This consequently increased the risk of PROM in both mice and humans. Inhibition of Ehf expression was observed with the introduction of EV-miR-155, resulting in a reduction in E-cadherin transcription in AECs. The activation of the β-catenin/Tcf7 complex by EV-miR-146a was observed to facilitate the transcription of Snail, MMP-9, and miR-146a/155, thereby inducing EMTs in AECs. The EMT was followed by AEC disruption of the intercellular junctions, leading to the formation of intercellular gaps. This phenomenon ultimately culminates in the deterioration of the biomechanical properties of the amnion, resulting in rupture of the amniotic membrane.

Materials and methods

Ethics statement

This study was performed in strict accordance with the recommendations of the Institutional Animal Care and Use Committee of the Jining Medical University. All protocols were approved by the Committee on the Ethics of Animal Experiments at the Jining Medical University (License ID: 2018-jc-019). Human amniotic membranes and amniotic fluid were obtained from the Obstetrics Department of the Jining Medical University Affiliated Hospital. Prior to participation, all participants provided written informed consent. This study was approved by the Clinical Ethics Committee of Jining Medical University (JNMC-2022-YX-153).

PROM model

One hundred mature inbred pregnant Kunming mice of specific pathogen-free grade, weighing 17–23 g, were used in this study. LPS was used to induce PROM as described previously [59]. LPS (100 μg/kg body weight) was injected intraperitoneally into mice at 15 d of pregnancy. PROM were observed after approximately 48 h of treatment. When bleeding was observed in the vagina, the uterus and embryos were isolated under aseptic conditions without breaking water. The CS model employed pregnant mice (ED-17), and the NL model experienced full-term birth (approximately 20 days). The amnion and amniotic fluid were analyzed for the expression of specific genes and compared with those from cesarean sections.

Isolation and culture of AECs in vitro

The methodology for isolating amniotic epithelial cells was based on established protocols from existing literature and further refined [60–62]. Initially, the amnion layer was manually separated from the chorion and washed with PBS lacking calcium and magnesium to remove any blood. To extract AECs, the amniotic membrane was incubated at 37 °C with a solution containing 0.25% trypsin and 0.02% EDTA. Cells released during the initial 5-minute digestion period were disregarded to remove debris. Cells from the subsequent two 20-minute digestion periods were combined and washed thrice

with PBS. The digestion was terminated by adding fetal bovine serum (FBS: PAN Biotech, Aidenbach, Germany). Subsequently, the cell suspensions were combined and filtered through a 70-μm cell strainer. Centrifugation of the cells was carried out at 1000 × g for 10 min to harvest the amniotic epithelial cells (AECs). Notably, approximately 95% of the isolated AECs exhibited positive staining for cytokeratins, validating their identity and purity to a significant extent. The isolated single AECs from the amnion were used as fresh AECS in this study. For cell culture, the cells were seeded in culture dishes at a density of 1×10^4 cells per cm^2 in a complete medium. The complete medium consisted of Dulbecco's Modified Eagle Medium/Nutrient Mixture F-12 (DMEM/F12; Gibco, Carlsbad, CA, USA) supplemented with 10% FBS, 10 ng/mL epidermal growth factor (Peprotech, Rocky Hill, TX, USA), 10 ng/mL basic fibroblast growth factor (Peprotech), and 55 μM β-mercaptoethanol (Sigma-Aldrich, St. Louis, MO, USA). To identify the mesenchymal phenotypes of the AECs, 15 ng/mL TGF-β (Peprotech) was added for 48 h [63].

Isolation and culture of F4/80-positive cells

The amniotic fluid from the CS model in pregnant mice underwent centrifugation at 5000 rpm for 30 min to isolate and harvest various cells, including macrophages, amniotic fluid stem cells, fibroblasts, and other cells. The collected cells were then resuspended in 500 μL DMEM, blocked with 4% BSA at room temperature for 15 min, and incubated with FITC-labeled F4/80 antibody for 1 h at room temperature to detect the proportion of macrophages. Subsequently, the magnetic bead separation for F4/80 positive cell enrichment Macrophages were isolated from the amniotic fluid via positive magnetic isolation and cultured in primary macrophage culture medium (SAIOS, PM-011, China) until they reached 80% confluence and were then harvested using 10 mM EDTA. The resulting cells were identified as M0 macrophages. For M1 polarization of macrophages, lipopolysaccharide (LPS; 1 μg/mL, Sigma, L4391, USA) and inerferon-γ (INF-γ, 20 ng/mL, Peprotech, 315-05, USA) were added in cell cultures for 48 h. To isolate EVs, FBS was replaced with the knockout serum replacement.

EMT analysis of the amnion and AECs

Amnions from LPS-induced PROM, natural labor (NL), cesarean section (CS), and EV-treated models were sectioned, dewaxed, rehydrated, blocked for endogenous peroxidase activity, and processed for antigen retrieval. The sections were blocked with 10% normal goat serum and incubated with mouse anti-E-cadherin and rabbit anti-N-cadherin primary antibodies (Abcam, USA) at 4 °C overnight, followed by a 2-hour incubation at room temperature with FITC/Cy5-conjugated goat anti-mouse/rabbit secondary antibody. After counterstaining with DAPI, images were captured using a TE-2000-E confocal microscope (Nikon, Yokohama, Japan). Fresh AECs were lysed using lysing matrix D (MP, USA) and a mammalian protein extraction kit (CWBio, China) to extract total proteins. Protein concentrations were determined using the BCA method (CW Bio, China). Western blot analysis was performed to detect the expression levels of E-cadherin, N-cadherin, and GAPDH in the fresh AECs. To examine the impact of various factors on the epithelial-to-mesenchymal transition of AECs, a variety of miRNAs and their targets were introduced into the AECs via transfection. The transfected AECs were then lysed, and the levels of EMT-related proteins, including E-cadherin, N-cadherin, Snail, β-catenin, Numb, Ehf, and MMP-9, were assessed using Western blot analysis. To ensure comparability across groups, a consistent total protein amount of 15 ug was loaded onto each sample, and identical exposure times were applied for the same markers across different samples.

Analysis of recruited macrophages in the uterus

The uteri were obtained from aborted mice treated with LPS and normal pregnant mice using the "swiss roll" method [64]. The sections were stained with hematoxylin and eosin for histological analysis. F4/80, a macrophage marker, was used to mark and count macrophages in the uterus using immunohistochemistry. Positive cells were counted and analyzed using Image J/IHC Profiler Tools [65].

Extracellular vesicles isolation and characterization

Each mouse yielded an average of ten embryos, and the amniotic fluid from each sac was pooled, yielding approximately 1 ml per mouse. Extracellular vesicles within the amniotic fluid were isolated through ultracentrifugation, adhering to the protocols established by the International Society for Extracellular Vesicles (ISEV) [66]. First, the freshly obtained amniotic fluid was diluted with PBS at a ratio of 1:7, and subjected to centrifugation at 800 × *g* for 5 min at 4 °C to eliminate cells, followed by centrifugation at 2,000 × *g* for 10 min and 10,000 × *g* for 30 min at 4 °C to remove cellular debris. Dilution of the cell culture supernatant with PBS is unnecessary, as it can be subjected to direct centrifugation to eliminate cells and cell debris. Subsequently, the supernatant was subjected to ultracentrifugation at 100,000 × *g* for 2 h at 4 °C using a Beckman Coulter Optima XPN-100 Ultracentrifuge equipped with a SW 41 Ti rotor. The supernatant was discarded, and the pellet was washed with 12 mL PBS. This was followed by a second ultracentrifugation at 100,000 × *g* for 2 h at 4 °C. The resulting supernatant was discarded, and the EVs were resuspended in 100 μL of PBS. Purified EVs were characterized using electron

microscopy, NTA (NanoSight LM10), and immunoblot analysis as described previously [67]. Protein concentrations in the EV preparations were determined using the BCA method (CWBio, China).

Microarray analysis

Analyses using the Agilent Mouse miRNA (8 × 60 K) array and the SBC Mouse (4 × 180 K) ceRNA array were performed by the National Engineering Center for Biochips (Shanghai, China). All data were analyzed using the SBC Analysis System (online tool for microarray analysis, http://sas.ebioservice.com/portal/root/molnet_shbh/index.jsp) to identify the differentially expressed genes [68]. The significance of the differential expression was assessed using the Student's t-test. Fold changes of ≥ 2 and a p-value of < 0.05 were used as the thresholds. Heat maps were generated using the Java TreeView software.

Luciferase reporter assay

Firefly luciferase reporter genes were constructed using the pCL3.0-Luc vector (Promega, Madison, WI, USA) and target sequences. A mutation was generated at positions 3–5 of the seed sequence using a QuikChange Mutagenesis Kit (Stratagene, USA). The 293T cells were transfected using Lipofectamine 3000 (Invitrogen) with a mixture of 1 mg/mL firefly luciferase reporter plasmid, 20 nM miRNA precursor or control, and 20 ng/mL *Renilla reniformis* luciferase-encoding plasmid (pRL-TK; Promega). Cells without the transfected precursor served as controls for normalization, and luciferase activity was measured 48 h post-transfection using a dual luciferase assay system. All assays were independently repeated at least three times.

Real-time PCR

The miRNAs were isolated using the miRcute miRNA Isolation Kit (Tiangen, Beijing, China). The cDNA was synthesized using a high-capacity RNA-to-cDNA Kit (Tiangen, Beijing, China). Real-time PCR was performed using SYBR PCR Mix (SYBR Green; Tiangen, Beijing, China) and primers for miR-146a, miR-1931, and miR-760-5p (Tiangen Biotech Co., Ltd.) in a Light Cycler 480 PCR system (Roche, USA). An external control (exosomes) (Tiangen) or U6 small nuclear RNA (cells) was used for normalization. For mRNA analysis, total RNA was extracted using the TRIzol reagent and reverse-transcribed using sequence-specific reverse transcription-PCR primers (Takara, China). PCR was performed using an RNA PCR Kit ver 3.0 (Takara). Specific primers for mRNAs and an endogenous control (GAPDH) were synthesized by Sangon Biotech (Shanghai, China). Gene expression was detected using a LightCycler 480 PCR system. Each experiment was performed in duplicate in 96-well plates and repeated thrice.

Coimmunoprecipitation and western blot analyses

Following transfection of AECs with a Myc-tagged Numb overexpression vector using Lipofectamine 3000, the cells were subsequently exposed to either 20 μm MG132 or 100nM Baf A1, after which the AECs were harvested. Coimmunoprecipitation assays were described previously [69]. AECs were lysed in 1 mL of lysis buffer containing 1× Complete Protease Inhibitor Cocktail (CWBio, Beijing, China). The lysates were centrifuged, and primary antibodies were added to 500 μL of the supernatant according to the manufacturer's instructions. For immunoprecipitation, an equal mixture of protein A and G Sepharose (Thermo Scientific, USA) was incubated with the lysate/antibody mixture for 2 h. For western blot, the immunoprecipitated mixture were analyzed using primary antibodies against β-catenin, Histone H3, and GAPDH. Horseradish peroxidase-coupled immunoglobulin IgGs was used as secondary antibody.

Biotin miRNA pull-down assay

The Biotin miRNA pull-down procedure was conducted utilizing the PureBinding® RNA-Protein Pull-Down Kit (GENESEED, China). A total of 1×10^7 cells or 1×10^{10} EVs were introduced into 1 × capture buffer, which included 10 μL of RNase inhibitor and 10 μL of protease inhibitor. The mixtures were thoroughly blended and subjected to ice-cold cracking for 10 min. Magnetic bead pretreatment and probe incubation with magnetic beads were performed according to the manufacturer's guidelines. The treated magnetic bead probe was added to the lysis mixture and rotated at 10 rpm for 1 h. Upon completion of the reaction, the mixture was placed on a magnetic rack to remove the supernatant. Subsequently, 1 mL of the Wash Buffer working solution was added to the collected magnetic beads and vortexed for 1 min. The supernatant was discarded on a magnetic rack. This washing step was repeated three times and the resulting magnetic beads were collected. The obtained product should be combined with loading buffer, denatured at 100°C for 15 min, and subsequently subjected to western blot analysis to detect the expression of PTBP1 and NONO. Biotinylated poly(G) (5′-GGGGGGGGGGGGGGGGGGGG-3′) was used as a negative control.

Loading of siRNAs or miRNAs into EVs

The EVs were subjected to two washes in Cytoporation® Media T (BTXpress, USA), followed by the combination of 1×10^{10} particles EVs with 50 μg siRNAs or miRNAs containing a 2′-O-methyl modification on each nucleotide and 3′ phosphorothioate internucleotide linkages at the first three 5′ and 3′ nucleotides (Genepharma, China) in 100 μL Cytoporation® Media T. Electroporation was performed at 400 V using a 2-mm electroporation cuvette (BTXpress). EVs were subsequently purified from

the mixture, and any unloaded siRNAs were eliminated using a SuperEV 0.5 purification column (Rengen Biosciences, China).

Tracking of EVs in vitro and in vivo

To visualize the influence of EVs on the AECs or human amniotic membrane in vitro, EVs were labeled with 2 μM Dil (Coolaber, China), for 1 h at 37 °C and then purified with a SuperEV 0.5 purification column. The EVs were then incubated with AECs or human amniotic membranes at different concentrations. The fluorescence intensity of Dil in the AECs or human amniotic membranes was assessed using a Leica TCS-SP8 confocal microscope and ImageJ software. To track EVs in vivo, they were labeled with 2 μM DiR (Absin, China) for 1 h at 37 °C and then purified with SuperEV 0.5 purification column. EVs were then injected intrauterine into mice at different concentrations. Then, 24 h after injection, the mice were anesthetized and imaged using an NIR-n Imaging System H (Series III 900/1700, NIROPTICS, Suzhou, China).

Human amniotic membrane and amniotic fluid

In this study, samples of amniotic membrane and amniotic fluid were procured from a cohort of gravida diagnosed with PROM due to vaginal infections ($n = 10$), and the amniotic membrane and amniotic fluid were collected immediately after elective cesarean section. The participants were selected based on specific criteria, including age range (25–30 years), the absence of any underlying diseases or genetic predispositions, and a gestational age of < 36 weeks. Furthermore, amniotic membrane and amniotic fluid samples were obtained from gravidas who underwent cesarean section at 36 weeks of gestation due to breech presentation and umbilical cord knot, and this served as a control group representing normal amniotic tissue and fluid ($n = 10$). The control participants were also within the specified age range (25–30 years) and had no underlying diseases or genetic histories. Amniotic and choroidal tissues were separated by blunt dissection. To ensure consistency at the collection site, the membrane was cut approximately 1 cm from the placental disc, excluding the area above the lower uterine pole and cervix. Subsequently, the membranes were washed with PBS to remove cellular debris and blood. To measure Young's modulus, the sample size was approximately 2 cm × 2 cm. Total proteins from the human amniotic membrane tissue samples from both PROM and normal cases were extracted and subjected to western blot analysis to determine EMT marker expression. Human CD14-positive cells were isolated from normal amniotic fluid using CD14-positive magnetic beads. These cells were then cultured in primary macrophage culture medium (SAIOS, PM-011, China). Positively sorting cells were confirmed to be hM0 macrophages. The polarization method for hM1 macrophages is consistent between humans and mice. hM0-EVs and hM1-EVs were isolated from the supernatants of hM0 or hM1 macrophages by ultracentrifugation. To investigate the role of hM0- or hM1-EVs in EMT normal human alveolar macrophages (AM) were cultured in suspension in DMEM supplemented with 5% FBS. Subsequently, 1×10^8 particles/mL of hM0-EVs or hM1-EVs was added separately and incubated for 48 h, with no EV treatment serving as a control. Western blot and immunofluorescence were used to detect EMT markers.

Young's modulus detection in the amniotic membrane

The Young's modulus of the amniotic membrane was determined using a Bruker Dimension FastScan AFM (BRUKER FastScan Bio, Germany). First, tweezers were used to carefully retrieve the amniotic membrane (1 cm^2 for mice, 2 cm^2 for humans) and position it on the coverslip. Subsequently, a suitable quantity of PBS was introduced and overlaid on a glass slide, exerting pressure to ensure a level surface. The upper coverslip and surplus water were eliminated. The tissue border was affixed to the amniotic membrane surface using Henkel instant adhesive (25637), ensuring its stability and flatness. We delineated a circular boundary around the tissue edge using a waterproof pen. PBS was applied to the tissues and transferred to a surgical instrument table. The 12 μm polystyrene microsphere probe position was then elevated to a superior level relative to the tissue to make appropriate modifications to the instrument parameters, and execute the instrument operation until the detection process was completed. The original data were analyzed using the NanoScope Analysis software (version 1.8) to obtain the torque curve and Young's modulus. Nine fetal amniotic membranes were obtained from each pregnant mouse to measure the properties of the murine amnion. Nine pieces of amniotic tissue were collected from each parturient woman to determine the lowest Young's moduli in the human amnion.

Transmission electron microscopy

To conduct morphologic observation of EVs, a 10 μL volume of EVs with a concentration of 1×10^8 particles/mL was deposited onto a copper grid for a precipitation period of 1 min, after which the supernatant was removed. Subsequently, a 10 μL solution of uranyl acetate was deposited onto the copper grid for a precipitation period of 1 min, followed by the removal of the supernatant. The samples were air-dried at room temperature for 10 min and examined with TEM (JEM1400, JEOL, Japan) at an acceleration voltage of 100 kV. To analyze cell connectivity, the amniotic membrane tissue was initially fixed with a 2.5% glutaraldehyde solution. Subsequently,

the tissue was subjected to a series of procedures, including dehydration, drying, coating, and imaging. The intercellular distance among the amniotic membrane epithelial cells was measured using the tools provided by the ImageJ software.

Statistical analysis

All experiments were independently performed at least three times and repeated in triplicate. Results are presented as the mean ± standard error of the mean (SEM). Differences were assessed using the Student's t-test (two groups) or one-way ANOVA (more than two groups), unless noted otherwise. $p < 0.05$. significant. A schematic illustration was drawn using the FigDraw tools (www.figdraw.com).

Supplementary Information

The online version contains supplementary material available at https://doi.org/10.1186/s12951-025-03192-6.

Supplementary Material 1

Supplementary Material 2

Author contributions

Gao Y. performed cell isolation and culture, obtained EVs, FCM, western blotting and drafted the manuscript. Zhang Y. collected human fetal membranes and amniotic fluid. Ming N. prepared the mice model and human amniotic membrane, performed PCR and IF. Miao W, Zhang J, Liu Y, Li Z, Song J performed EVs isolation, biological analysis, and western blotting. Bai C. designed the experiments, and reviewed the manuscript, Li X and Guan W participated in its design and coordination.

Funding

This research was supported by the National Natural Science Foundation of China (Grant No. 82471729), Research Fund for Academician Lin He New Medicine (Grant No.JYHL2022ZD05).

Data availability

The microarray data generated in this study have been deposited in the Gene Expression Omnibus (GEO) repository (accession numbers GSE149296, GSE149630, and GSE150066).

Declarations

Competing interests

The authors declare no competing interests.

Received: 23 January 2024 / Accepted: 1 February 2025
Published online: 04 March 2025

References

1. Chen HN, et al. PDLIM1 stabilizes the E-Cadherin/beta-Catenin complex to prevent epithelial-mesenchymal transition and metastatic potential of Colorectal Cancer cells. Cancer Res. 2016;76(5):1122–34.
2. Hwang WL, et al. MicroRNA-146a directs the symmetric division of snail-dominant colorectal cancer stem cells. Nat Cell Biol. 2014;16(3):268–80.
3. Musavi Shenas SMH, et al. SiRNA-mediated silencing of Snail-1 induces apoptosis and alters micro RNA expression in human urinary bladder cancer cell line. Artif Cells Nanomed Biotechnol. 2017;45(5):969–74.
4. Saxen L, Thesleff I. Epithelial-mesenchymal interactions in murine organogenesis. Ciba Found Symp. 1992;165:183–93. discussion 193-8.
5. Ilancheran S, et al. Stem cells derived from human fetal membranes display multilineage differentiation potential. Biol Reprod. 2007;77(3):577–88.
6. Azargoon A, Negahdari B. Lung regeneration using amniotic fluid mesenchymal stem cells. Artif Cells Nanomed Biotechnol. 2018;46(3):447–51.
7. Bai C, et al. MiR-15/16 mediate crosstalk between the MAPK and Wnt/beta-catenin pathways during hepatocyte differentiation from amniotic epithelial cells. Biochim Biophys Acta Gene Regul Mech. 2019;1862(5):567–81.
8. Gao Y, et al. Long non-coding RNA maternally expressed 3 increases the expression of Neuron-Specific genes by targeting mir-128-3p in All-Trans Retinoic Acid-Induced Neurogenic differentiation from amniotic epithelial cells. Front Cell Dev Biol. 2019;7:342.
9. Gao Y, et al. Combination of melatonin and Wnt-4 promotes neural cell differentiation in bovine amniotic epithelial cells and recovery from spinal cord injury. J Pineal Res. 2016;60(3):303–12.
10. Mogami H, et al. Healing of Preterm ruptured fetal membranes. Sci Rep. 2017;7(1):13139.
11. Mano Y, et al. Tocilizumab inhibits interleukin-6-mediated matrix metalloproteinase-2 and– 9 secretions from human amnion cells in preterm premature rupture of membranes. Gynecol Obstet Invest. 2009;68(3):145–53.
12. Richardson LS, Taylor RN, Menon R. Reversible EMT and MET mediate amnion remodeling during pregnancy and labor. Sci Signal, 2020. 13(618).
13. Janzen C, et al. The role of epithelial to mesenchymal transition in human amniotic membrane rupture. J Clin Endocrinol Metab. 2017;102(4):1261–9.
14. El-Shazly S, et al. Increased expression of pro-inflammatory cytokines in placentas of women undergoing spontaneous preterm delivery or premature rupture of membranes. Am J Reprod Immunol. 2004;52(1):45–52.
15. Heijnen HF, et al. Activated platelets release two types of membrane vesicles: microvesicles by surface shedding and exosomes derived from exocytosis of multivesicular bodies and alpha-granules. Blood. 1999;94(11):3791–9.
16. Jiang N, et al. Exosomes mediate epithelium-mesenchyme crosstalk in Organ Development. ACS Nano. 2017;11(8):7736–46.
17. Ogawa Y, et al. Exosome-like vesicles with dipeptidyl peptidase IV in human saliva. Biol Pharm Bull. 2008;31(6):1059–62.
18. Lobb RJ, et al. Optimized exosome isolation protocol for cell culture supernatant and human plasma. J Extracell Vesicles. 2015;4:27031.
19. Jeronimo C, Henrique R. Is There a Role for Exosome-derived MicroRNAs in Detection of Renal Cell Tumors Using Urine Samples? Editorial to [European Urology Focus 2/2 (2016) 210–218]. Eur Urol Focus, 2016. 2(6): pp. 654–655.
20. Xie J, et al. The relationship between amniotic fluid miRNAs and congenital obstructive nephropathy. Am J Transl Res. 2017;9(4):1754–63.
21. Wei M, et al. Malignant ascites-derived exosomes promote proliferation and induce carcinoma-associated fibroblasts transition in peritoneal mesothelial cells. Oncotarget. 2017;8(26):42262–71.
22. Kong FL et al. The role of exosomes derived from cerebrospinal fluid of spinal cord injury in neuron proliferation in vitro. Artif Cells Nanomed Biotechnol. 2018;46(1):200–5
23. Maroto R, et al. Effects of storage temperature on airway exosome integrity for diagnostic and functional analyses. J Extracell Vesicles. 2017;6(1):1359478.
24. Hesari A et al. Tumor-derived exosomes: potential biomarker or therapeutic target in breast cancer?. J Cell Biochem. 2018;119(6):4236–40.
25. Salomon C, et al. Placental exosomes as early biomarker of Preeclampsia: potential role of exosomal MicroRNAs across Gestation. J Clin Endocrinol Metab. 2017;102(9):3182–94.
26. Santangelo A et al. A microRNA signature from serum exosomes of patients with glioma as complementary diagnostic biomarker. J Neurooncol. 2018;136(1):51–62.
27. Sheller-Miller S et al. Exosomes cause Preterm Birth in mice: evidence for Paracrine signaling in pregnancy. Sci Rep. 2019;9(1):608.
28. Menon R et al. Differences in cord blood extracellular vesicle cargo in preterm and term births. Am J Reprod Immunol, 2022. 87(3).
29. Ramos BRA et al. Circulating Extracellular vesicles microRNAs are altered in women undergoing Preterm Birth. Int J Mol Sci, 2023. 24(6).
30. Dixon CL, et al. Amniotic fluid Exosome Proteomic Profile exhibits Unique pathways of Term and Preterm Labor. Endocrinology. 2018;159(5):2229–40.
31. Shahin HI, et al. Microvesicles and exosomes released by amnion epithelial cells under oxidative stress cause inflammatory changes in uterine cells. Biol Reprod. 2021;105(2):464–80.
32. Sutton L, Mason DY, Redman CW. HLA-DR positive cells in the human placenta. Immunology. 1983;49(1):103–12.
33. Mann M, et al. An NF-kappaB-microRNA regulatory network tunes macrophage inflammatory responses. Nat Commun. 2017;8(1):851.

34. Li B, et al. miR-146a modulates autoreactive Th17 cell differentiation and regulates organ-specific autoimmunity. J Clin Invest. 2017;127(10):3702–16.
35. Xu YH, et al. Exosomal mir-155-5p drives widespread macrophage M1 polarization in hypervirulent -induced acute lung injury via the MSK1/p38-MAPK axis. Volume 28. Cellular & Molecular Biology Letters; 2023. 1.
36. Chen SX, et al. ETS2 overexpression ameliorates cartilage injury in osteoarthritis by the ETS2/miR-155/STAT1/DNMT1 feedback loop pathway. Volume 1866. Biochimica Et Biophysica Acta-Gene Regulatory Mechanisms; 2023. 4.
37. Cheng X, et al. Numb mediates the interaction between wnt and notch to modulate primitive erythropoietic specification from the hemangioblast. Development. 2008;135(20):3447–58.
38. Fossum SL, et al. Ets homologous factor regulates pathways controlling response to injury in airway epithelial cells. Nucleic Acids Res. 2014;42(22):13588–98.
39. Zhao TS, et al. ESE3 inhibits pancreatic Cancer metastasis by upregulating E-Cadherin. Cancer Res. 2017;77(4):874–85.
40. Xu P, Alfaidy N, Challis JRG. Expression of matrix metalloproteinase (MMP)-2 and MMP-9 in human placenta and fetal membranes in relation to preterm and term labor. J Clin Endocrinol Metabolism. 2002;87(3):1353–61.
41. Farre D, et al. Identification of patterns in biological sequences at the ALGGEN server: PROMO and MALGEN. Nucleic Acids Res. 2003;31(13):3651–3.
42. Khan A et al. JASPAR 2018: update of the open-access database of transcription factor binding profiles and its web framework. Nucleic Acids Res. 2018;46(D1):D260–6.
43. Hessvik NP, Llorente A. Current knowledge on exosome biogenesis and release. Cell Mol Life Sci. 2018;75(2):193–208.
44. Qin X, et al. Exosomal miR-196a derived from cancer-associated fibroblasts confers cisplatin resistance in head and neck cancer through targeting CDKN1B and ING5. Genome Biol. 2019;20(1):12.
45. Cook KB, et al. RBPDB: a database of RNA-binding specificities. Nucleic Acids Res. 2011;39:D301–8.
46. Record M, et al. Exosomes as new vesicular lipid transporters involved in cell-cell communication and various pathophysiologies. Biochim Biophys Acta. 2014;1841(1):108–20.
47. Liu Q, et al. Donor dendritic cell-derived exosomes promote allograft-targeting immune response. J Clin Invest. 2016;126(8):2805–20.
48. Borges FT, et al. TGF-beta1-containing exosomes from injured epithelial cells activate fibroblasts to initiate tissue regenerative responses and fibrosis. J Am Soc Nephrol. 2013;24(3):385–92.
49. Xiao H, et al. Mast cell exosomes promote lung adenocarcinoma cell proliferation - role of KIT-stem cell factor signaling. Cell Commun Signal. 2014;12:64.
50. Qian B, et al. M1 macrophage-derived exosomes impair beta cell insulin secretion via mir-212-5p by targeting SIRT2 and inhibiting Akt/GSK-3β/β-catenin pathway in mice. Diabetologia. 2021;64(9):2037–51.
51. Liu SJ et al. M1-like macrophage-derived exosomes suppress angiogenesis and exacerbate cardiac dysfunction in a myocardial infarction microenvironment. Basic Res Cardiol. 2020. 115(2).
52. van Roy F, Berx G. The cell-cell adhesion molecule E-cadherin. Cell Mol Life Sci. 2008;65(23):3756–88.
53. Guo X, et al. Regulation of adherens junctions and epithelial paracellular permeability: a novel function for polyamines. Am J Physiology-Cell Physiol. 2003;285(5):C1174–87.
54. Ojakian GK, Ratcliffe DR, Schwimmer R. Integrin regulation of cell-cell adhesion during epithelial tubule formation. J Cell Sci. 2001;114(5):941–52.
55. Last JA, et al. Determining the mechanical properties of human corneal basement membranes with atomic force microscopy. J Struct Biol. 2009;167(1):19–24.
56. Chaurasia SS et al. Effect of Fibrin Glue on the Biomechanical Properties of Human Descemet's Membrane. PLoS ONE, 2012. 7(5).
57. Benson-Martin J, et al. The Young's modulus of fetal preterm and term amniotic membranes. Eur J Obstet Gynecol Reproductive Biology. 2006;128(1–2):103–7.
58. Bhunia S et al. New approaches suggest term and preterm human fetal membranes may have distinct biomechanical properties. Sci Rep, 2022. 12(1).
59. Hirsch E, Saotome I, Hirsh D. A model of intrauterine infection and preterm delivery in mice. Am J Obstet Gynecol. 1995;172(5):1598–603.
60. International Society for Stem Cell Research. Current protocols in stem cell biology. Hoboken: Wiley, N.J.; 2009.
61. Miki T, Strom SC. Amnion-derived pluripotent/multipotent stem cells. Stem Cell Rev. 2006;2(2):133–41.
62. Miki T, et al. Stem cell characteristics of amniotic epithelial cells. Stem Cells. 2005;23(10):1549–59.
63. Richardson LS, Taylor RN, Menon R. Reversible EMT and MET mediate amnion remodeling during pregnancy and labor. Science Signaling, 2020. 13(618).
64. Bao Y, et al. PRSS8 suppresses colorectal carcinogenesis and metastasis. Oncogene. 2019;38(4):497–517.
65. Varghese F, et al. IHC profiler: an open source plugin for the quantitative evaluation and automated scoring of immunohistochemistry images of human tissue samples. PLoS ONE. 2014;9(5):e96801.
66. Théry C et al. Minimal information for studies of extracellular vesicles 2018 (MISEV2018): a position statement of the International Society for Extracellular Vesicles and update of the MISEV2014 guidelines. J Extracell Vesicles, 2018. 7(1).
67. Li J, et al. Exosomes mediate the cell-to-cell transmission of IFN-alpha-induced antiviral activity. Nat Immunol. 2013;14(8):793–803.
68. Tusher VG, Tibshirani R, Chu G. Significance analysis of microarrays applied to the ionizing radiation response. Proc Natl Acad Sci U S A. 2001;98(9):5116–21.
69. Yang Y et al. GPR40 modulates epileptic seizure and NMDA receptor function. Sci Adv, 2018. 4(10).

Publisher's note

Springer Nature remains neutral with regard to jurisdictional claims in published maps and institutional affiliations.